

A high-performance GRAB sensor reveals differences in the dynamics and molecular regulation between neuropeptide and neurotransmitter release

Received: 10 July 2024

Accepted: 8 January 2025

Published online: 18 January 2025

 Check for updates

Xiju Xia^{1,2,3} & Yulong Li^{1,2,3,4} 

The co-existence and co-transmission of neuropeptides and small molecule neurotransmitters within individual neuron represent a fundamental characteristic observed across various species. However, the differences regarding their in vivo spatiotemporal dynamics and underlying molecular regulation remain poorly understood. Here, we develop a GPCR-activation-based (GRAB) sensor for detecting short neuropeptide F (sNPF) with high sensitivity and spatiotemporal resolution. Furthermore, we investigate the in vivo dynamics and molecular regulation differences between sNPF and acetylcholine (ACh) from the same neurons. Interestingly, our findings reveal distinct spatiotemporal dynamics in the release of sNPF and ACh. Notably, our results indicate that distinct synaptotagmins (Syt) are involved in these two processes, as Syt7 and Syt α for sNPF release, while Syt1 for ACh release. Thus, this high-performance GRAB sensor provides a robust tool for studying neuropeptide release and shedding insights into the unique release dynamics and molecular regulation that distinguish neuropeptides from small molecule neurotransmitters.

Neurons typically utilize two primary classes of signaling molecules for transmitting information: small molecule neurotransmitters, responsible for fast synaptic transmission, and neuromodulators, predominantly involved in slow, non-synaptic transmission^{1,2}. Neuropeptides represent the most diverse group of neuromodulators in the human body, encompassing more than 100 distinct types, and they exert their functions through G protein-coupled receptors (GPCRs)^{3–5}. Neuropeptides and small molecule neurotransmitters are typically stored in large dense-core vesicles (LDCVs) and synaptic vesicles (SVs)⁶, respectively, which likely have distinct properties that govern their activity-dependent release^{3,7,8}. Early studies have demonstrated that the neuropeptide and the small molecule neurotransmitter induced slow and fast excitatory postsynaptic potential,

respectively, in sympathetic ganglia⁹. Interestingly, the presence of both neuropeptides and small molecule neurotransmitters in the same neuron is a common phenomenon in almost all neurons across a wide range of species^{3,4,7,10}, providing a diverse set of modulatory mechanisms capable of operating on distinct spatial and/or temporal scales, thereby enabling complex behaviors such as the flight response, sleep, learning, and social behaviors^{5,8,9,11–14}. However, the majority of previous studies have examined the release of neuropeptides and the release of small molecule neurotransmitters in isolation, within different cell types; therefore, the potential similarities and/or differences in their spatiotemporal dynamics and the molecular mechanisms regulating their release within the same neuron remain poorly understood.

¹State Key Laboratory of Membrane Biology, School of Life Sciences, Peking University, Beijing, China. ²PKU-IDG/McGovern Institute for Brain Research, Beijing, China. ³Academy for Advanced Interdisciplinary Studies (AAIS), and Peking University–Tsinghua University–National Institute of Biological Sciences Joint Graduate Program (PTN), Peking University, Beijing, China. ⁴Chinese Institute for Brain Research, Beijing, China.  e-mail: yulongli@pku.edu.cn

Drosophila serves as an excellent model organism for studying the regulation of neuropeptides and small molecule neurotransmitters in vivo due to its less redundant genome compared to mammals, as well as its well-developed genetic tools and database^{15,16}. Short neuropeptide F (sNPF), a pivotal neuropeptide in *Drosophila*, plays a role in various physiological processes, including feeding, metabolism, sleep and glucose homeostasis^{17–22}. Notably, analyses from transcriptomics, immunocytochemistry and genetic driver lines have revealed the enrichment of sNPF, choline acetyltransferase (ChAT) and the vesicular ACh transporter (VAcHT) in Kenyon cells (KCs) of the *Drosophila* mushroom body (MB). This suggests the co-existence of the neuropeptide sNPF and the small molecule neurotransmitter ACh within the same KCs^{19,20,23–26}. These cells function as the olfactory learning center, and both sNPF and ACh have been shown to be important for learning and memory^{24,27,28}. Thus, KCs provide an ideal platform for studying the “co-transmission” of neuropeptide and small molecular neurotransmitter. Previously, we developed, characterized, and applied a G protein-coupled receptor (GPCR) activation-based (GRAB) ACh sensor (GRAB_{ACh3.0}, short as ACh3.0), in vivo in *Drosophila* studies^{29,30}; however, a comparable tool for the in vivo detection of sNPF release remains unavailable.

Several methods have been developed for detecting neuropeptide release in vivo, each with its own advantages and disadvantages. Microdialysis has been widely used to measure the dynamics of neuropeptide release in the mammalian brain³¹; however, this technique is invasive and has low spatiotemporal resolution due to the relatively large embedded probe (~200 μm diameter) and low sampling rate (requiring 5–10 min per sample). Alternatively, neuropeptides tagged with either a fluorescent protein or fluorogen-activating protein (FAP) have been used to track the release of neuropeptides or to monitor the fusion of LDCVs; examples include GFP-tagged rat atrial natriuretic peptide (ANP^{GFP})³², pHluorin-tagged neuropeptide Y (NPY-pHluorin)³³, the GCaMP6s-tagged rat atrial natriuretic peptide neuropeptide release reporter (NPRR^{ANP})³⁴, and FAP-tagged *Drosophila* insulin-like peptide 2 (Dilp2-FAP)³⁵, these reporters offer good cell specificity and sensitivity for neuropeptide detection in vivo. However, because the fluorescent tag is usually ~10–100 times larger than the neuropeptide itself in terms of molecular weight, these reporters do not necessarily reflect the true dynamics of endogenous neuropeptides. Another approach is to fuse the fluorescent tag to the luminal side of an LDCV-specific membrane protein such as cytochrome b561, providing a versatile tool for monitoring neuropeptide release; however, this approach lacks neuropeptide specificity³⁶. The Tango GPCR assay can also be used to detect neuropeptide release in vivo, but requires a relatively long time for reporter expression and is irreversible^{37–39}. Finally, CNiFER (cell-based neurotransmitter fluorescent engineered reporter) biosensors require the implantation of genetically modified cells, making it highly invasive and lacking cell type specificity^{40–44}.

Recently, taking advantage of a similar strategy, our group and others have independently developed several series of genetically encoded fluorescent sensors for detecting small molecule neurotransmitters and mammalian neuropeptides with high specificity and spatiotemporal resolution^{29,45–63}. Capitalizing on the scalability of this approach, we therefore develop a GRAB sensor for detecting the in vivo dynamics of sNPF in *Drosophila*. By expressing both the sNPF and ACh sensors in KCs in the *Drosophila* MB and performing in vivo two-photon imaging, we measure the spatiotemporal dynamics of both sNPF and ACh release in real time. We discover that sNPF release shows distinct spatiotemporal dynamics with ACh release, while both sNPF and ACh release require neuronal synaptobrevin (nSyb). To elucidate the molecular underpinnings of sNPF and ACh release, we conduct CRISPR/Cas9-based screening of the synaptotagmin family in the KCs, revealing that sNPF release is primarily mediated by Syt7 and Syt8, while ACh release is mainly mediated by Syt1.

Results

Development and characterization of GRAB_{sNPF} sensors

To generate a GRAB sensor for detecting sNPF (GRAB_{sNPF}), we initially replaced the third intracellular loop (ICL3) of the sNPF receptor (sNPF_R) with the ICL3-circularly permuted EGFP (cpEGFP) module from the well characterized norepinephrine sensor GRAB_{NE1m}⁴⁸ (Fig. 1a). Given the high conservation of the sNPF peptide sequence among Diptera, which includes flies and mosquitoes⁴⁹ (Supplementary Fig. 1a), we selected the sNPF_R from *Culex*, *Aedes* and *Drosophila* for our studies^{64,65}. For each sNPF_R backbone, we generated a library by inserting the cpEGFP module in to different positions within intracellular loop 3 (ICL3) of the GPCR (Supplementary Fig. 1b). We subsequently expressed candidate sensors in HEK293T cells and examined their maximum brightness and fluorescence change ($\Delta F/F_0$) in response to application of 1 μM sNPF. Unless specified otherwise, we utilized the *Drosophila* sNPF2 neuropeptide (WFGDVNQKPIRSPSLRLRFa), known for its physiological functions and a higher potency in activating *Drosophila* sNPF_R^{66–68}. The most promising candidate was identified based on the *Culex quinquefasciatus* sNPF_R, exhibiting the highest response and relatively high brightness. We named this sensor GRAB_{sNPF_{0.1}} and utilized it for further optimization (Fig. 1b and Supplementary Fig. 1a, b). Following optimization of the replacement sites, performing site-directed mutagenesis on cpEGFP and linker sequences between cpEGFP and the GPCR, we obtained GRAB_{sNPF_{0.0}}, exhibiting a peak $\Delta F/F_0$ of ~350% in response to sNPF application (Fig. 1c and Supplementary Fig. 1c, d). Structural data suggested that D287^{6.59} serves as a predicted binding site between NPY and its receptor Y_{1R}, a vertebrate paralog of sNPF_R^{64,69}. Based on this insight, we developed an sNPF-insensitive sensor, GRAB_{sNPF_{mut}} by introducing the arginine mutagenesis in the corresponding site D302^{6.59} in GRAB_{sNPF_{0.0}} (Fig. 1c and Supplementary Fig. 1d). When expressed in HEK293T cells, GRAB_{sNPF_{0.0}} traffics to the plasma membrane (Fig. 1d) and has a concentration-dependent increase in fluorescence in response to sNPF, with an EC₅₀ of 64 nM (Fig. 1e); in contrast, GRAB_{sNPF_{mut}} showed non-detectable response to sNPF across all concentrations tested (Fig. 1e).

We then characterized the specificity, spectral properties, and kinetics of GRAB_{sNPF_{0.0}} expressed in HEK293T cells. GRAB_{sNPF_{0.0}} has high specificity for sNPF, with virtually no response elicited by a wide range of neuropeptides and small molecule neurotransmitters (Fig. 1f). Moreover, according to the previous studies, four forms of sNPF were predicted on the precursor gene (CG13968): sNPF1 (AQRSPSLRLRFa), sNPF2 (WFGDVNQKPIRSPSLRLRFa), sNPF3 (KPQLRLWa) and sNPF4 (KPMRLR_{Wa})^{15,70}. However, subsequent mass spectrometric studies of *Drosophila* CNS tissue and midgut extracts revealed that these peptides are not processed as predicted. The major bioactive peptide is a truncated form sNPF1^{4–11} (SPSLRLRFa), which is the same sequence as sNPF2^{12–19}. In addition, the peptide sNPF3 and sNPF4 occur as KPQLRLWa and KPMRLR_{Wa}^{71–74}. Besides of that, three major sNPF isoforms are also reported in mosquitos, which showed high similarity in sequences of that in *Drosophila*⁶⁴. Next, we test the dose-dependent curve of GRAB_{sNPF_{0.0}} in response to all of these isoforms. The results showed that GRAB_{sNPF_{0.0}} can detect all these sNPF analogs and homologs from *Drosophila* and *Culex*, with similar peak responses but with EC₅₀ values ranging from 23 nM to 1.7 μM , among them, sNPF1^{4–11} showed similar response to sNPF1 and sNPF2. (Supplementary Fig. 2a–c). We characterized one-photon spectral properties of GRAB_{sNPF_{0.0}}, determining peak excitation and emission wavelengths of 505 nm and 520 nm, respectively (Fig. 1g), as well as a two-photon excitation peak at 930 nm (Supplementary Fig. 2d). With respect to the sensor's activation kinetics, we measured an average rise time constant (τ_{on}) ranges from 0.23 to 1.42 s and an average decay time constant (τ_{off}) ranges from 2.99 to 4.18 s upon local application of sNPF, we also estimated a rate constant for sNPF of $k_{\text{on}} = 421 \text{ s}^{-1} \mu\text{M}^{-1}$ for GRAB_{sNPF_{0.0}} (Fig. 1h). Finally, we confirmed that GRAB_{sNPF_{0.0}} shows no detectable

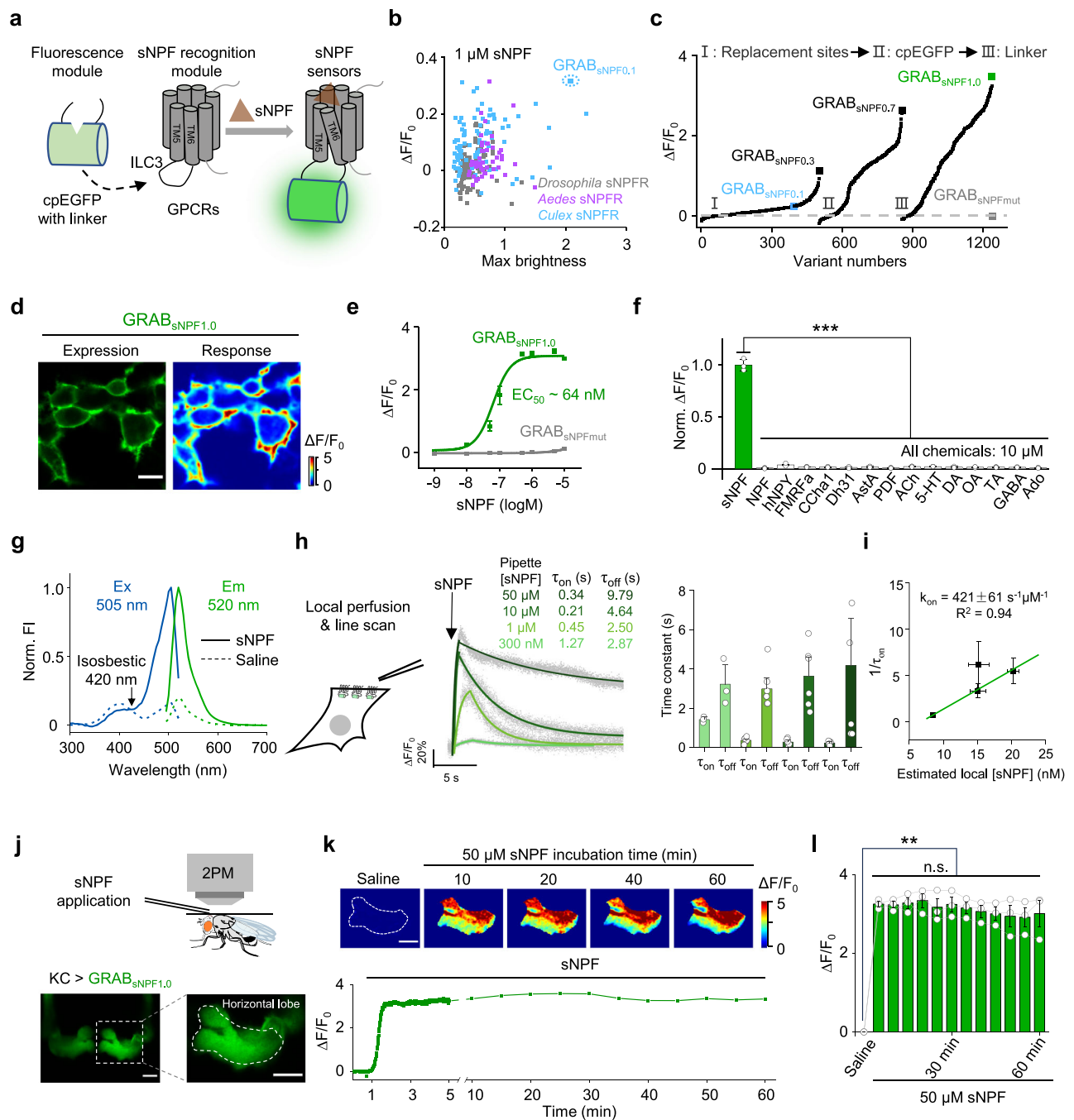


Fig. 1 | Development and characterization of GRAB_{sNPF} sensors. **a** Schematic diagram depicting the principle of GRAB_{sNPF}. **b** Replacements sites screening of GRAB_{sNPF} prototype from three libraries. Each library is generated by inserting the cpEGFP module in to different positions within intracellular loop3 (ICL3) of indicated GPCR. **c** Optimization steps of GRAB_{sNPF} (Top). Various candidates' responses to sNPF (Bottom). **d** Representative image of GRAB_{sNPF1.0} expression and response to sNPF in HEK293T cells. **e** Dose–response curves of GRAB_{sNPF1.0} and GRAB_{sNPFmut}; $n = 3$ wells, with an average 300 cells per well. **f** Normalized $\Delta F/F_0$ of GRAB_{sNPF1.0}; $n = 3$ wells, with an average 300 cells per well. sNPF short neuropeptide F, NPF Neuropeptide F, hNPY human neuropeptide Y, FMRFa FMRFamide, CCHa1 CCHa-mide 1, Dh31 diuretic hormone 31, AstA allatostatin A, PDF pigment-dispersing factor, ACh acetylcholine, 5-HT 5-hydroxytryptamine, DA dopamine, OA octopamine, TA tyramine, GABA gamma-aminobutyric acid, Ado adenosine. One-way ANOVA followed by Tukey's multiple-comparison test, $F_{14,30} = 769.35$, $P = 2.41 \times 10^{-34}$. Post hoc test: $P = 0$ for sNPF versus other compounds. **g** One-photon

spectra of GRAB_{sNPF1.0} in the absence and presence of sNPF. FI, fluorescence intensity. **h** On and off kinetics for GRAB_{sNPF1.0}. Illustration of the local puffing system (left), Representative response trace (middle), group summary of τ_{on} and τ_{off} (Right); $n = 3/7/6/6$ cells for 300 nM, 1 μ M, 10 μ M, 50 μ M from 3 cultures. **i** The association rate constant of the GRAB_{sNPF1.0} for sNPF. Local sNPF concentrations were estimated from **h**. **j** Schematic illustration (top) and fluorescence images (bottom) of GRAB_{sNPF1.0} expression in MB KCs. $n = 3$ flies. **k** Representative pseudocolor images (top) and trace (bottom) of GRAB_{sNPF1.0} in response to sNPF. **l** Summary peak $\Delta F/F_0$ of GRAB_{sNPF1.0}. $n = 3$ flies. One-way repeated measures ANOVA followed by Tukey's multiple-comparison tests, $F = 369.31$, $P = 2.7 \times 10^{-3}$. Post hoc test: Specific p values corresponding to this figure are reported in the Source Data. Scale bar in **d**, 10 μ m; Scale bar in **j**, **k**, 25 μ m. Data are shown as mean \pm s.e.m. in **e**, **f**, **h**, **i**, **l**, with the error bars or shaded regions indicating the s.e.m. *** $P < 0.001$, ** $P < 0.01$, and n.s. not significant.

downstream coupling by measuring G protein-dependent pathways and β -arrestin recruitment, although wild-type *Culex* sNPF activated both signaling pathways in response to sNPF (Supplementary Fig. 2e, f).

Next, we evaluated the ability of GRAB_{sNPF_{FL0}} to detect sNPF *in vivo* by expressing GRAB_{sNPF_{FL0}} in KCs in the *Drosophila* MB via R13F02-Gal4. Using two-photon imaging, we then measured the fluorescence change of GRAB_{sNPF_{FL0}} in response to sNPF application (Fig. 1i). Application of 50 μ M sNPF induced a robust increase in GRAB_{sNPF_{FL0}} fluorescence that was stable for at least 60 min (Fig. 1j, k), suggesting that GRAB_{sNPF_{FL0}} can reliably measure the dynamics of sNPF *in vivo*, and showing that GRAB_{sNPF_{FL0}} is suitable for long-term imaging.

GRAB_{sNPF} reports endogenous sNPF release *in vivo*

Then, we examined whether GRAB_{sNPF_{FL0}} can detect the release of endogenous sNPF. We pan-neuronally expressed GRAB_{sNPF_{FL0}} under the control of nSyb-Gal4, with a primary focus on the fluorescent change in MB, as previous studies have demonstrated high sNPF expression in KCs in the *Drosophila* MB^{20,75}. We found that high K⁺ induced an increase in GRAB_{sNPF_{FL0}} fluorescence in the horizontal lobe of MB (Fig. 2a–c). In contrast, no significant response to high K⁺ was measured in GRAB_{sNPF_{FL0}}-expressing sNPF-knockout (sNPF-KO) flies. However, the exogenous application of sNPF still elicited a robust response in these flies, confirming the sensor expression and functionality was unaffected (Fig. 2b, c). These results indicated that GRAB_{sNPF_{FL0}} could detect the endogenous sNPF release specifically. Furthermore, besides the mushroom body (MB), sNPF is also expressed in other brain regions, such as the fan-shaped body²⁰. To test whether GRAB_{sNPF_{FL0}} can detect sNPF release in fan-shaped body, we expressed GRAB_{sNPF_{FL0}} with sNPF-Gal4, and successfully observed the fluorescence increase upon high K⁺ application (Supplementary Fig. 3a–c). In addition, we proceeded to examine whether GRAB_{sNPF_{FL0}} could detect the release of sNPF in response to physiological stimuli. To address this, we expressed GRAB_{sNPF_{FL0}} in the *Drosophila* MB (R13F02-Gal4-driven) and found that repeated odorant application induced a time-locked increase in GRAB_{sNPF_{FL0}} fluorescence in the horizontal lobe (Supplementary Fig. 3d–g). In contrast, no detectable response to same odorant application was observed in flies expressing GRAB_{sNPF_{mut}} (Supplementary Fig. 3f, g).

Next, to achieve cell autonomous and temporally precise control over endogenous sNPF release in KCs, we employed CsChrimson to activate KCs, and measured sNPF release in response to optogenetic activation⁷⁶ in the axonal region (i.e., the horizontal lobe) (Fig. 2d, e) and the dendritic region (i.e., the calyx) (Supplementary Fig. 4a) of KCs *in vivo*. Our findings revealed that optogenetic stimulation evoked time-locked and pulse number-dependent sNPF release in both regions (Fig. 2f–h and Supplementary Fig. 4a–c). In contrast, no detectable response was observed in GRAB_{sNPF_{mut}} expressed flies (Fig. 2g). The rise time constant (τ_{on}) in the axonal and dendritic regions were found to range from 2.1–26.9 s and 4.3–19.9 s, respectively, with time constants correlated with increasing pulse numbers in both regions (Fig. 2h and Supplementary Fig. 4d). Interestingly, the rising phase of the GRAB_{sNPF_{FL0}} signal was optimally described by a double-exponential function, reflecting the existence of both a rapid rising phase and a relatively slow rising phase (Fig. 2i–k and Supplementary Fig. 4e–g).

Taken together, these results indicate that GRAB_{sNPF_{FL0}} can specifically detect the endogenous sNPF release and is suitable to study the spatiotemporal dynamics of sNPF release *in vivo*.

GRAB sensors reveal spatially distinct patterns of sNPF and ACh release from KCs

Numerous neurons—including KCs in the *Drosophila* MB—synthesize and release both neuropeptides and small molecule neurotransmitters. To compare their spatiotemporal dynamics, we therefore

optogenetically activated KCs in the MB and measured the release patterns of sNPF and ACh. Specifically, we expressed either GRAB_{sNPF_{FL0}} or the ACh sensor ACh3.0⁷⁹ along with CsChrimson in KCs (Fig. 3a). To avoid potential interference induced by activating other neurons through ACh release, we included the nicotinic ACh receptor blocker mecamylamine (Meca) throughout these experiments. We found that optogenetic stimulation of KCs induced sNPF release in the horizontal lobe, calyx, and soma regions; in contrast, ACh release was restricted to the horizontal lobe and calyx regions (Fig. 3b–e and Supplementary Fig. 5a–d). As a control, similar response of ACh3.0 was induced by ACh application in soma and calyx regions (Supplementary Fig. 5e–g). In addition, the levels of both sNPF release and ACh release from the horizontal lobe were significantly higher compared to their release from the calyx (Fig. 3e). Taken together, these results indicate that sNPF and ACh exhibit distinct release patterns in the soma region of KCs.

GRAB sensors reveal distinct activity-dependent dynamics underlying sNPF and ACh release

Having shown the differences in the spatial release patterns between sNPF and ACh, we proceeded to investigate whether differences exist in calcium sensitivity and the temporal dynamics of their release. Although it is widely accepted that neuropeptide release is generally slower than that of small molecule neurotransmitter⁷⁷, this has not been examined directly by measuring the release of these two types of signaling molecules within the same cell type *in vivo*. Given that axons exhibited a higher release levels compared to other neuronal compartments (Fig. 3e), we examined the kinetics and temporal profiles of sNPF and ACh release in the horizontal lobe in flies expressing CsChrimson together with either GRAB_{sNPF_{FL0}} or ACh3.0 (Fig. 4a). We found that light pulses generated an GRAB_{sNPF_{FL0}} signal that had slower rise and decay kinetics (τ_{on} : 0.94–4.4 s; τ_{off} : 4.9–7.2 s) compared to that of the ACh3.0 signal (τ_{on} : 0.13–0.24 s; τ_{off} : 1.1–1.4 s) (Fig. 4b–g). Given that the activation kinetics of GRAB_{sNPF_{FL0}} and ACh3.0 sensors are 0.23–1.42 s (Fig. 1h) and 0.10–0.29 s²³, respectively, when compared to the ACh signal, the physiologically slower kinetics of the sNPF signal induced by optogenetic stimulations suggest a distinction between the release of neuropeptides and small molecule neurotransmitters from the same neurons.

Furthermore, our findings revealed that the release of sNPF required high intensity stimulation since the peak GRAB_{sNPF_{FL0}} signal showed the light pulse frequency-dependent manner (Fig. 4b), whereas the peak ACh3.0 signal was largely unaffected by stimulation frequency (Fig. 4d). Additionally, the release of both sNPF and ACh exhibited a positive correlation with calcium signal. However, the slopes of these correlations were distinct, suggesting a significant disparity in their calcium sensitivity (Supplementary Fig. 6).

Delivery of multiple stimuli within a short interval can result in either an enhancement or depression of neurotransmitter or neuro-modulator release relative to the response induced by the initial stimulus⁷⁸. This phenomenon, known as short-term plasticity, plays a role in various physiological functions and pathological conditions, including learning, memory and some psychiatric disorders^{78,79}. To further test the short-term plasticity, we examined the release pattern of sNPF and ACh and found that applying more light pulses at a fixed frequency (1 Hz) potentiated the GRAB_{sNPF_{FL0}} signal, but depressed the ACh3.0 signal (Supplementary Fig. 7a–d), suggesting post-tetanic potentiation of neuropeptide release. In addition, when we applied a stimulation protocol consisting of repeated trains of light pulses, the results showed that sNPF release was potentiated during this stimulation protocol (Supplementary Fig. 7e), while ACh release was attenuated (Supplementary Fig. 7f). Furthermore, to mitigate the interference from off kinetics of the sensors, we decreased the stimulation intensity to ensure that the signal returned to baseline before the next stimulation. Our results demonstrated that GRAB_{sNPF_{FL0}} signal

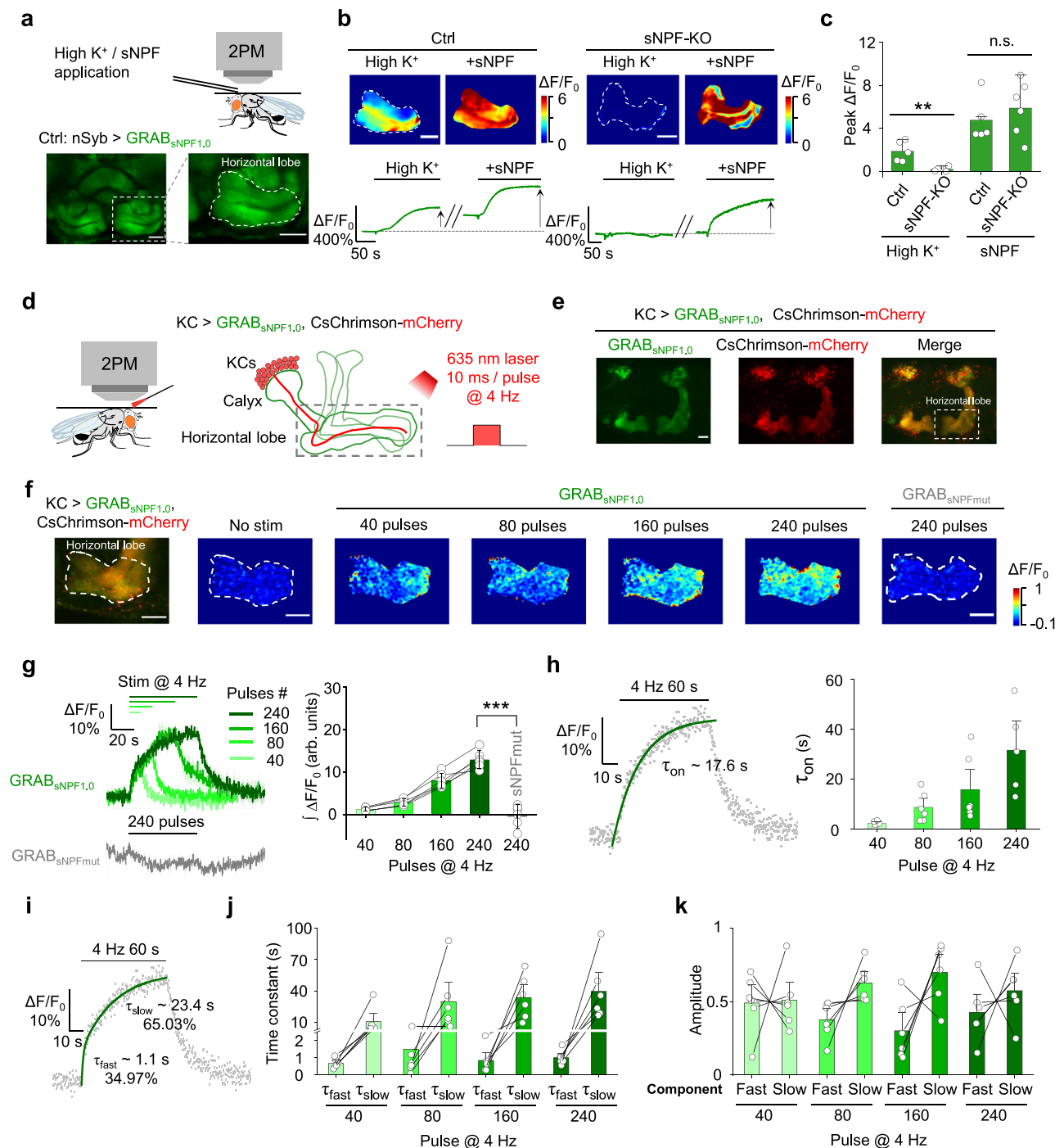


Fig. 2 | The GRAB_{SNPF1.0} sensor can detect sNPF release in vivo. **a** Schematic diagram (top) and representative fluorescence images (bottom) of GRAB_{SNPF1.0} expressed in the horizontal lobe in the *Drosophila* MB. $n = 5$ flies. **b** Representative pseudocolor images (top) and traces (bottom) of GRAB_{SNPF1.0} expressed in control flies (left) and sNPF KO flies (right); where indicated, high K⁺ and sNPF were applied. **c** Summary of peak $\Delta F/F_0$ measured in the indicated flies in response to high K⁺ and sNPF; $n = 5$ flies for Ctrl, $n = 6$ flies for sNPF-KO. Two-tailed Student's t tests, High K⁺: $P = 1.99 \times 10^{-3}$ for Ctrl versus sNPF-KO, sNPF: $P = 0.45$ for Ctrl versus sNPF-KO. **d** Schematic illustration depicting the experimental setup. CsChrimson-mCherry and GRAB_{SNPF1.0} were expressed in KCs in the *Drosophila* MB, and 635-nm laser light pulses were used to optogenetically activate the KCs. **e** Representative fluorescence images of GRAB_{SNPF1.0} and CsChrimson-mCherry in the MB; the horizontal lobe is indicated by the dashed white box. $n = 6$ flies. **f** Fluorescence image of GRAB_{SNPF1.0} and CsChrimson-mCherry in the horizontal lobe in KCs (left-most image) and

representative pseudocolor images (right) of the fluorescence responses of GRAB_{SNPF1.0} and GRAB_{SNPFmut} to the indicated number of 635-nm laser pulses applied at 4 Hz. $n = 6$ flies. **g** Traces (left) and summary (right) of the fluorescence responses of GRAB_{SNPF1.0} and GRAB_{SNPFmut}; $n = 6$ flies each. Two-tailed Student's t tests, $P = 2.15 \times 10^{-8}$ for GRAB_{SNPF1.0} versus GRAB_{SNPFmut}. **h** GRAB_{SNPF1.0} fluorescence was measured before, during, and after a 240-pulse train of 635-nm light. The rise phase was fitted with a single-exponential function (left), and the time constants (τ_{on}) are summarized on the right; $n = 6$ flies. **i** GRAB_{SNPF1.0} fluorescence was measured before, during, and after a 240-pulse train of 635-nm light, and the rise phase was fitted with a double-exponential function. Summary of the fast and slow time constants (**j**) and relative amplitudes (**k**) measured as shown in **i**; $n = 6$ flies. All Scale bar, 25 μm . Data are shown as mean \pm s.e.m. in **c**, **g**, **h**, **j**, **k**, with the error bars or shaded regions indicating the s.e.m. *** $P < 0.001$, ** $P < 0.01$, and n.s. not significant.

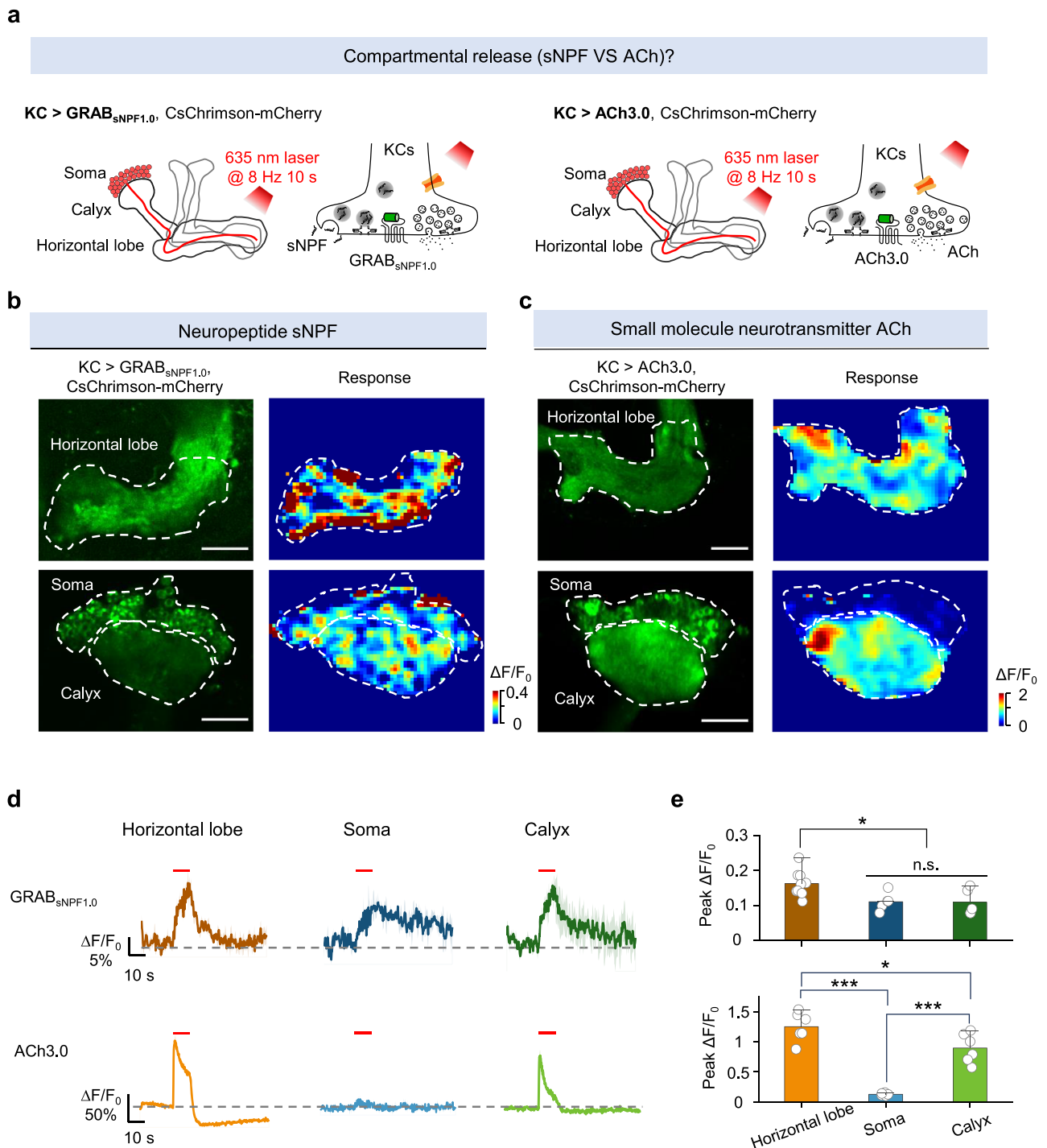
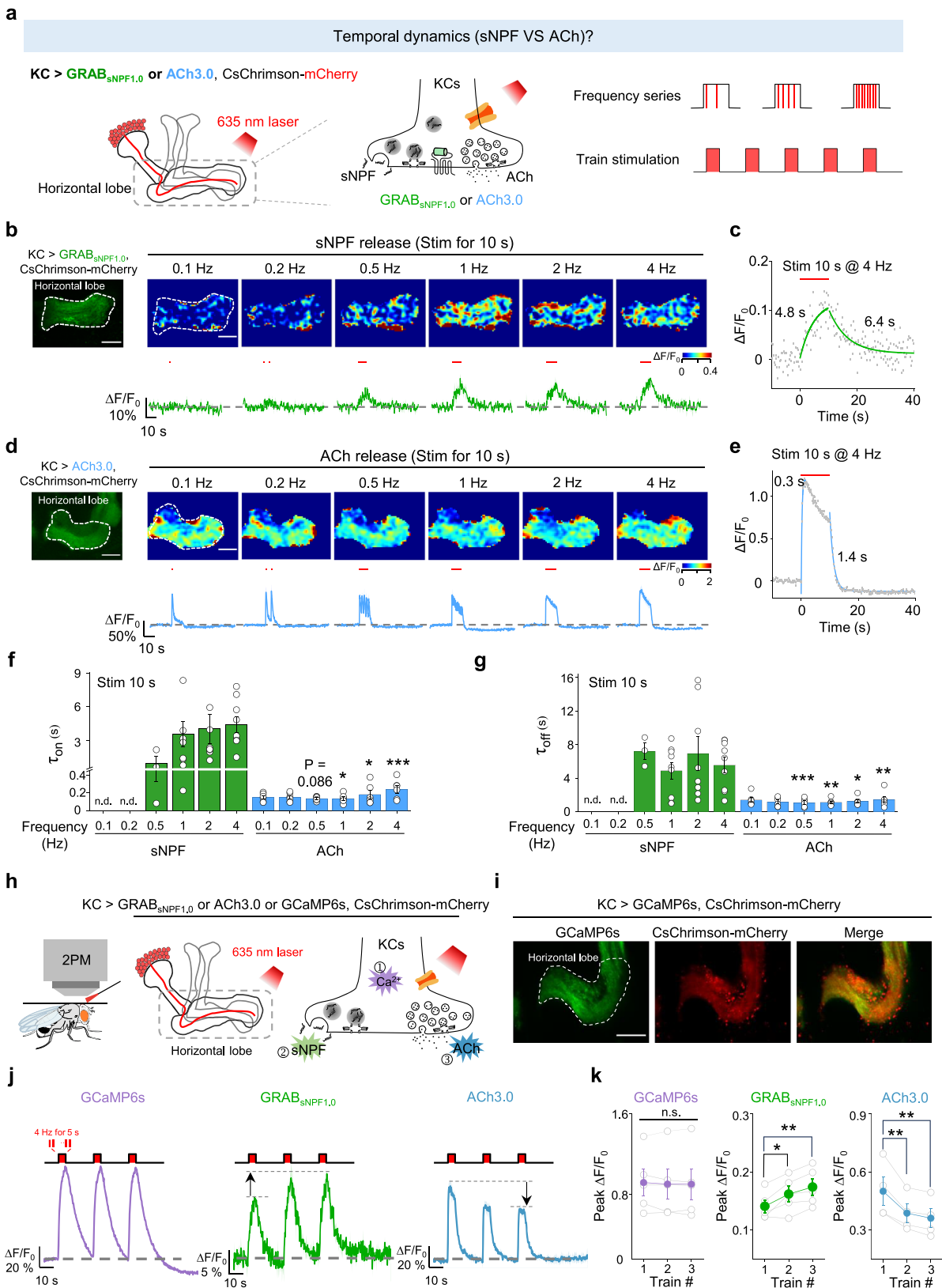


Fig. 3 | The GRAB_{sNPF1.0} and ACh3.0 sensors reveal spatial difference in release between sNPF and ACh. **a** Schematic diagram depicting the KC regions in the *Drosophila* MB, which can be divided into the axon (horizontal lobe), dendrite (calyx), and soma regions. Also shown is the strategy for imaging sNPF and ACh release in the MB using GRAB_{sNPF1.0} and ACh3.0, respectively. The 100 μ M nAChR antagonist mecamylamine (Meca) was present throughout these experiments. Representative fluorescence images (left columns) and pseudocolor images (right columns) showing the change in GRAB_{sNPF1.0} (**b**) and ACh3.0 (**c**) fluorescence in response to 80 light pulses delivered at 8 Hz. The top rows show the horizontal lobe, and the bottom rows show the calyx and soma regions (dashed outlines). $n = 5$ flies for GRAB_{sNPF1.0} and ACh3.0. Scale bars, 25 μ m. Representative traces (**d**) and

quantification (**e**) of the change in GRAB_{sNPF1.0} (**d**, top) and ACh3.0 (**d**, bottom) fluorescence in response to 80 light pulses delivered at 8 Hz. GRAB_{sNPF1.0}: $n = 9$ flies for Horizontal lobe, $n = 5$ flies for Soma and Calyx; ACh3.0: $n = 6$ flies for Horizontal lobe and Calyx, $n = 5$ flies for Soma. A one-way analysis of variance (ANOVA) followed by Tukey's multiple-comparison tests, GRAB_{sNPF1.0}: $P = 0.04$ for Horizontal lobe versus Soma, $P = 0.04$ for Horizontal lobe versus Calyx, and $P = 1$ for Soma versus Calyx; ACh3.0: $P = 1.0 \times 10^{-6}$ for Horizontal lobe versus Soma, $P = 0.03$ for Horizontal lobe versus Calyx, and $P = 7.26 \times 10^{-5}$ for Soma versus Calyx. Data are shown as mean \pm s.e.m. in **d**, **e**, with the error bars or shaded regions indicating the s.e.m. *** $P < 0.001$, * $P < 0.05$, and n.s. not significant.



still exhibit potentiation, whereas ACh3.0 signal displayed depression. Moreover, calcium levels remained stable throughout this process (Fig. 4h–k).

Taken together, the above results suggest that the release of sNPF required high intensity stimulation whereas the release of ACh was significant under low intensity stimulation. Furthermore, sNPF release

exhibits slower kinetics compared to ACh release and shows distinct short-term plasticity with ACh release.

To further validate the distinct dynamics of sNPF and ACh release, we performed dual-color imaging to simultaneously detect the release of sNPF and ACh using GRAB_{sNPF1.0} and a red fluorescent ACh indicator GRAB_{rACh0.5} (Referred as rACh1.4 in previous studies⁸⁰, was similar to

Fig. 4 | The GRAB_{sNPF1.0} and ACh3.0 sensors reveal distinct activity-dependent properties for sNPF and ACh release. **a** Schematic diagram depicting the strategy. The 100 μ M nAChR antagonist mecamylamine (Meca) was present throughout these experiments. Representative fluorescence image (top left), pseudocolor images (top right), and traces (bottom right) of the change in GRAB_{sNPF1.0} (**b**) and ACh3.0 (**d**) fluorescence in response to the indicated light stimuli (red bars). Example traces showing response of GRAB_{sNPF1.0} (**c**) and ACh3.0 (**e**) under the indicated light stimuli; the rise and decay phases are each fitted with a single-exponential function. Summary of the rise (**f**) and decay (**g**) time constants (τ_{on} and τ_{off}) of GRAB_{sNPF1.0} and ACh3.0 fluorescence in response to the indicated light stimuli. $n = 3/9/8/9$ flies for GRAB_{sNPF1.0} at 0.5, 1, 2, 4 Hz; $n = 6$ flies for ACh3.0 at each frequency. Two-tailed Student's *t* tests, **f** GRAB_{sNPF1.0} versus ACh3.0: $P = 0.086$ for 0.5 Hz, $P = 0.03$ for 1 Hz, $P = 0.03$ for 2 Hz, and $P = 4.08 \times 10^{-4}$ for 4 Hz.

g GRAB_{sNPF1.0} versus ACh3.0: $P = 6.05 \times 10^{-5}$ for 0.5 Hz, $P = 0.009$ for 1 Hz, $P = 0.03$ for 2 Hz, and $P = 0.005$ for 4 Hz. **h** Schematic diagram illustrates the experimental design. **i** Representative fluorescent imaging showing expression of GCaMP6s (green) and CsChrimson-mCherry (red). $n = 5$ flies. **j, k** Representative traces and group summary of GCaMP6s, GRAB_{sNPF1.0} and ACh3.0 response to indicated stimulation. $n = 5$ flies for GCaMP6s and GRAB_{sNPF1.0}, $n = 4$ for ACh3.0. One-way repeated measures ANOVA followed by Tukey's multiple-comparison tests, GCaMP6s: $F = 39.34$, $P = 0.003$. GRAB_{sNPF1.0}: $F = 159.93$, $P = 2.25 \times 10^{-4}$. ACh3.0: $F = 54.3$, $P = 0.005$. Specific *p* values of Tukey's multiple-comparison corresponding to this figure are reported in the Source Data. All scale bars, 25 μ m. Data are shown as mean \pm s.e.m. in **b, d, h** and **i**, with the error bars or shaded regions indicating the s.e.m. *** $P < 0.001$, ** $P < 0.01$, and * $P < 0.05$, and n.s. not significant.

previously published green sensor ACh3.0 except that cpEGFP is replaced by cpmApple.) in the same fly. Firstly, we co-expressed GRAB_{sNPF1.0} and rACh0.5 in KCs and detected their signal under high K^+ stimulation (Supplementary Fig. 8a, b). The release of sNPF and ACh was observed upon high K^+ stimulation and the rise time of sNPF is significantly lower than that of ACh (Supplementary Fig. 8c, d). Secondly, to assess the release profiles of sNPF and ACh in response to varying stimulation intensities, we performed high K^+ stimulation at different concentrations. The results revealed that 7.5 mM K^+ induced sNPF signal was significantly lower than that induced by 15 mM K^+ stimulation, whereas ACh signal remained relatively consistent across both stimulation conditions (Supplementary Fig. 8e). All of this data is consistent with the results obtained using green sensors exclusively, further validating our findings.

GRAB_{sNPF1.0} and ACh3.0 sensors reveal that sNPF and ACh reside in vesicle pools with distinct properties

Vesicle pools play a critical role in presynaptic physiology, particularly with respect to release probability and determining synaptic strength, with their sizes dynamically adjusting in response to stimuli⁸¹. To evaluate the dynamics of the vesicle pools containing sNPF and ACh in KCs, we applied both continuous and trains of stimuli to activate KCs (Fig. 5a, b); as above, we included Meca throughout these experiments. Firstly, to examine the dynamics of vesicle pools in response to the long continuous stimuli, we applied a 40-pulse train, succeeded by a 30-min train of 7200 pulses, and followed by several brief stimuli applied at an increasing interval (Fig. 5c). We found that the GRAB_{sNPF1.0} signal initially decreased slightly but was relatively stable during the 30-min stimulation period and the subsequent brief stimuli, this is consistent with the calcium signal during the same stimulation (Fig. 5c, e and Supplementary Fig. 9). In contrast, the ACh3.0 signal decreased rapidly during the 30-min stimulation period, but recovered during the subsequent brief stimuli (Fig. 5d, f). These data suggest that sNPF resides in a large pool of releasable vesicles so that sNPF release can be maintained for a relatively long period; in contrast, ACh resides in a smaller releasable pool that can be depleted with a strong stimulation, but can replenish relatively quickly.

Next, to delve deeper into the dynamics of the vesicle pools containing sNPF and ACh during the discontinuous stimuli, we delivered 10 trains of light pulses with a 3-min interval while measuring sNPF or ACh release in the horizontal lobe (Fig. 5g). The results showed a relatively stable peak and integrated response for both sNPF and ACh release in response to these 10 trains (Fig. 5h–m). Such a relative stable response could be attributed to the vesicle pools recovering during each 3-min interval and/or the presence of a relatively large vesicle pool that can maintain release during intense stimulation.

GRAB sensors reveal that sNPF and ACh release are mediated by overlapping and distinct molecular mechanisms in flies

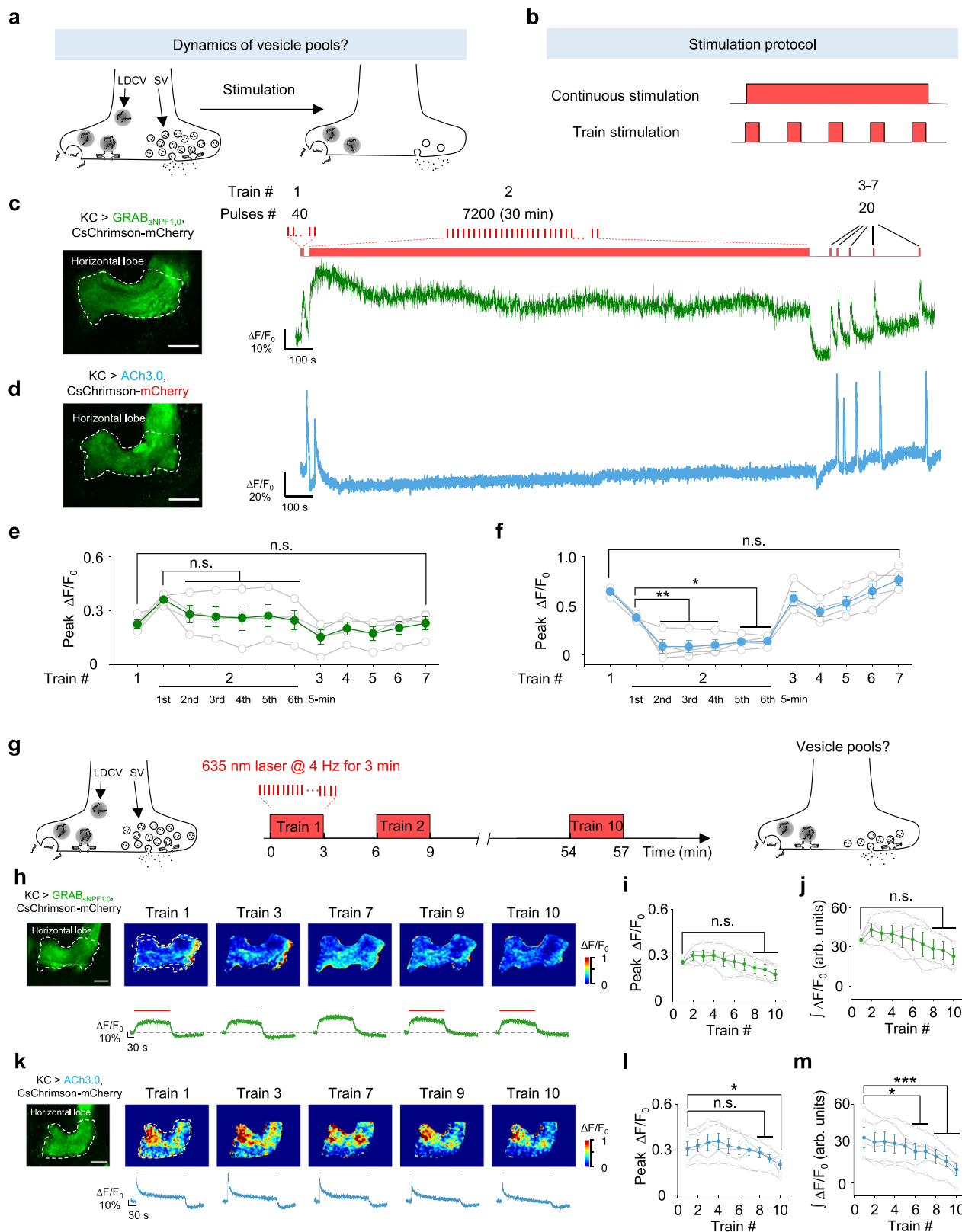
Both SVs and LDCVs require soluble N-ethylmaleimide-sensitive factor attachment receptor (SNARE) complexes for vesicle fusion^{82,83}. In

Drosophila, neuronal synaptobrevin (nSyb) is a core component of the SNARE complex and is indispensable for the release of small molecule neurotransmitters⁸⁴. In contrast, whether the same SNARE proteins mediate the release of both sNPF and ACh in the same neuron is an open question.

To determine whether nSyb mediates the release of ACh and/or sNPF in KCs, we expressed tetanus toxin light chain (Tetxlc) in KCs to specifically cleave nSyb⁸⁵ and then quantified the effect on ACh and sNPF release. We found that expressing Tetxlc significantly reduced both the high K^+ -induced GRAB_{sNPF1.0} signal (Fig. 6a) and the optogenetically induced ACh3.0 signal (Fig. 6b), but had no apparent effect on response induced by direct application of sNPF and ACh, respectively (Fig. 6a, b). Thus, both sNPF release and ACh release require nSyb.

Given that nSyb appears to play a role in the release of both sNPF and ACh, we proceeded to investigate the factors that account for the differences in the dynamics of release between sNPF and ACh. The release of neuropeptides and small molecule neurotransmitters (i.e., the fusion of LDCVs and SVs, respectively) is tightly regulated by calcium ions (Ca^{2+})⁸⁶, with synaptotagmins (Syts) serving as the Ca^{2+} sensor, ultimately triggering vesicle fusion^{86–88}. With respect to the release of small molecule neurotransmitters in SVs, the function of Syts such as Syt1 and Syt7 has been studied in detail in both vertebrates and invertebrates^{89–98}. In contrast to the limited studies on which Syt(s) mediate the release of neuropeptides in vitro, the in vivo regulation of neuropeptide release in large dense-core vesicles (LDCVs) remains undetermined.

Syts are a large family of membrane proteins, with seven isoforms present in *Drosophila*. Five of these isoforms—Syt1, Syt4, Syt7, Syt α , and Syt β —are predicted to bind Ca^{2+} and may therefore regulate the release of neuropeptides and/or small molecule neurotransmitters⁹⁹. To determine which Syt isoform(s) regulate neuropeptide release, we systematically knocked out each of these five Syt isoforms and then measured optogenetically induced sNPF release in KCs using the GRAB_{sNPF1.0} sensor. We utilized a cell type-specific CRISPR/Cas9-based strategy to knockout each Syt isoform in KCs¹⁰⁰. Based on this strategy, we generated sgRNA library lines targeting each *Drosophila* Syt isoform, with each isoform targeted by three sgRNAs in one fly line; control flies expressed Cas9 but no sgRNAs. We then performed an imaging screen to compare sNPF release in control flies with that in flies lacking specific Syt isoforms in KCs (Fig. 6c). We found that flies lacking either Syt7 or Syt α had significantly reduced sNPF release in response to optogenetic stimulation (Fig. 6c, e). Surprisingly, knocking out both Syt7 and Syt α did not show a synergistic effect on sNPF release, suggesting that these two Syt isoforms may function in the same pathway (Supplementary Fig. 10). Finally, we measured ACh release in flies lacking each Syt isoform and found that consistent with the previous studies, knocking out Syt1—but no other isoforms—significantly reduced ACh release (Fig. 6d, f). These results indicate that distinct Syt isoforms regulate different vesicle-release pathways in the same type of neurons, with Syt7 and Syt α mediating neuropeptide



release and Syt1 mediating the release of small molecule neurotransmitters (Fig. 6g).

Discussion

Here, we report the development, characterization, and in vivo application of GRAB_{sNPF1.0}, a high-performance genetically encoded green fluorescent sensor designed to detect the neuropeptide sNPF. This

high-performance sensor has high affinity for sNPF, along with high specificity, and high spatiotemporal resolution. When expressed in *Drosophila*, GRAB_{sNPF1.0} reliably detects the release of sNPF, with a biphasic release pattern during optogenetic stimulation consisting of a fast phase followed by a slow phase. Furthermore, we examined the spatiotemporal patterns of sNPF and ACh release from KCs and found that both sNPF and ACh are released from the horizontal lobe and

Fig. 5 | The GRAB_{sNPFL0} and ACh3.0 sensors reveal distinct pools of sNPF- and ACh-containing vesicles. Schematic diagram depicting the experimental strategy (a) and stimulation protocol (b) used to study the size of vesicle pools containing sNPF and ACh. The 100 μM nAChR antagonist mecamylamine (Meca) was present throughout these experiments. Representative fluorescence image (left) and traces (right) of GRAB_{sNPFL0} (c) and ACh3.0 (d) response to the indicated stimulation. Summary of peak $\Delta F/F_0$ of GRAB_{sNPFL0} (e) and ACh3.0 (f); $n = 4$ flies. One-way repeated measures ANOVA followed by Tukey's multiple-comparison tests. **e** $F = 39.63$, $P = 0.008$. **f** $F = 141.33$, $P = 1.28 \times 10^{-3}$. Specific p values of Tukey's multiple-comparison corresponding to this figure are reported in the Source Data. **g** Schematic diagram depicting the strategy for studying vesicle pools containing sNPF and ACh. **h, k** Representative fluorescence images (top left), pseudocolor images (top right), and traces (bottom right) of GRAB_{sNPFL0} (h) and ACh3.0 (k)

response to the indicated stimulation; $n = 4$ flies. Summary of the peak $\Delta F/F_0$ (i) and integrated $\Delta F/F_0$ (j) of GRAB_{sNPFL0} (h); $n = 4$ flies. One-way repeated measures ANOVA followed by Tukey's multiple-comparison tests. **i** $F = 68.75$, $P = 0.004$, post hoc test: $P = 0.97$, 0.83 , 0.26 for Train #1 versus Train #8, Train #9, Train #10. **j** $F = 35.25$, $P = 0.009$, post hoc test: $P = 0.97$, 0.93 , 0.49 for Train #1 versus Train #8, Train #9, Train #10. Summary of the peak $\Delta F/F_0$ (l) and integrated $\Delta F/F_0$ (m) of ACh3.0 (k); $n = 4$ flies. One-way repeated measures ANOVA followed by Tukey's multiple-comparison tests. **l** $F = 61.84$, $P = 0.0014$, post hoc test: $P = 0.99$, 0.41 , 0.02 for Train #1 versus Train #8, Train #9, Train #10. **m** $F = 17.12$, $P = 0.014$, post hoc test: $P = 0.02$, 0.02 , 5.01×10^{-4} , 1.09×10^{-5} , 5.64×10^{-8} for Train #1 versus Train #6, Train #7, Train #8, Train #9, Train #10. All scale bars, 25 μm . Data are shown as mean \pm s.e.m. in **e, f, i, j, l, m**, with the error bars or shaded regions indicating the s.e.m. *** $P < 0.001$, ** $P < 0.01$, * $P < 0.05$, and n.s. not significant.

calyx regions, while sNPF is also released from the soma and has slower kinetics compared to ACh release. Moreover, although both sNPF and ACh require nSyb for their release, our Syt knockout screen revealed that sNPF release is regulated by Syt α and Syt7, whereas ACh release is regulated by Syt1. These differences in Ca²⁺ sensors between sNPF and ACh release may therefore contribute to the observed differences in release kinetics between LDCVs and SVs in the same type of neurons.

Advantages of GRAB_{sNPFL0} and its potential applications and limitations

Recently, several GPCR-based neuropeptide sensors have been developed^{51,52,54,60–63}. Among these sensors, GRAB_{sNPFL0} exhibits comparable on kinetics and relatively fast off kinetics, and it demonstrates an average amplitude of response and affinity (Supplementary Table 1). Notably, to the best of our knowledge, GRAB_{sNPFL0} represents the first instance of a peptide GRAB sensor being utilized in *Drosophila*.

Furthermore, Our GRAB_{sNPFL0} sensor offers several advantages for detecting neuropeptide transmission compared to existing methods. First, this sensor can directly detect the release of endogenous sNPF, making it superior to fluorescent reporter protein-tagged neuropeptides such as ANP-GFP³², NPRR^{ANP38}, and Dilp2-FAP³⁵. Second, GRAB_{sNPFL0} has considerably better temporal resolution (τ_{on} 0.23–1.42 s; τ_{off} 2.99–4.18 s) compared to microdialysis, which is limited by its relatively slow sampling time (>5 min).

Importantly, GRAB_{sNPFL0} can be used to measure sNPF release in vivo with high specificity, sensitivity, and spatiotemporal resolution. Using GRAB_{sNPFL0}, we explore the dynamics of sNPF release in KCs. In addition to being released from KCs, sNPF can also be released from a wide range of neuron types, playing an important role in regulating various behaviors including circadian rhythms, glucose homeostasis, and body size^{17,18,20,21,68}. Moreover, sNPF plays an important role in many insects, including mosquitoes such as *Aedes aegypti*⁶⁴. Given that sNPF is highly conserved among insects, GRAB_{sNPFL0} could potentially be used in mosquitoes, such as, it could be utilized to monitor the dynamics of sNPF in mosquitoes during the feeding processes. Therefore, this high-performance sNPF sensor is suitable for various in vivo applications and has potential ability to measure sNPF release in a wide range of behavioral processes and species, providing valuable insights into the regulation of sNPF under a variety of physiological conditions.

Although our GRAB_{sNPFL0} possesses several advantages for detection of sNPF release both in vitro and in vivo, it is not without its limitations. Firstly, GRAB_{sNPFL0} is a green sensor, which restricts our ability to conduct multiplexed imaging of sNPF in conjunction with other green-fluorescent sensors. Secondly, GRAB_{sNPFL0} is an intensity-based sensor, which presents significant challenges for performing absolute quantitative measurements. Future studies into the development of red-shift protein-based and fluorescence lifetime-based sensors may provide a viable solution to circumvent these constraints.

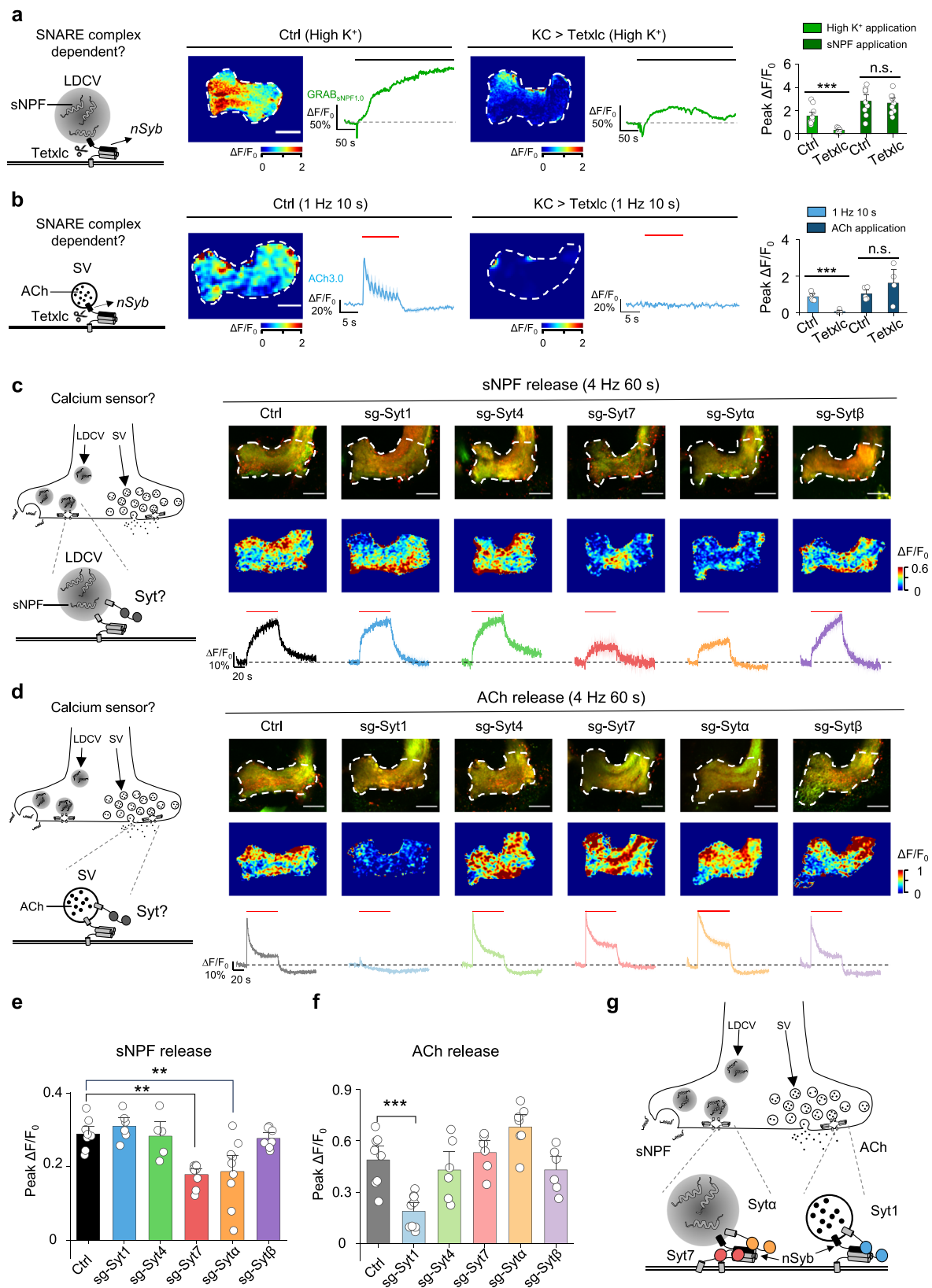
Spatiotemporal dynamics of neuropeptide and small molecule neurotransmitter release from the same type of neurons

The ability of individual neurons to release both neuropeptides and small molecule neurotransmitters is a core feature of neuronal signaling. Our findings reveal that, in contrast to ACh, sNPF can be released from the soma. This observation was not surprising, given that the somatic release of neuropeptides has been reported in both vertebrates^{52,101} and invertebrates¹⁰². In *Drosophila*, the somatic release of neuropeptides has been implicated in regulating rhythmic behaviors¹⁰². This also fits well with structural analyses of neuropeptide release sites in EM sections¹⁰³. Moreover, our results suggested that the on kinetics of the release of sNPF in vivo are slower than those of ACh based on the comparable in vitro on kinetics of GRAB_{sNPFL0} and ACh3.0, which is consistent with the relatively slower fusion of neuropeptide-containing LDCVs compared to neurotransmitter-containing SVs¹⁰⁴. It also correlated well with the slow and fast excitatory postsynaptic potential induced by the neuropeptide and small molecule neurotransmitter respectively⁹. According to previous literature¹⁰⁵, different Syt isoforms are known to have different kinetic properties, as Syt1 displayed the fastest disassembly kinetics with Ca²⁺, while Syt7 exhibited the slowest disassembly kinetics. Thus, the observed difference in release kinetics of sNPF and ACh may be attributed to the intrinsic kinetics of distinct Syt. In addition, we found that sNPF release can be maintained for a longer duration than ACh release, suggesting key differences in their respective vesicle pools and indicating that neuropeptides can have broader, longer-lasting effects than small molecule neurotransmitters.

Even after several decades of research, understanding the patterns of neural activity required to drive the release of both neuropeptides and small molecule neurotransmitters from a single neuron continues to be an enigmatic challenge. Fluorescence sensors can greatly facilitate the analysis of these patterns by detecting the release of neuropeptides and small molecule neurotransmitters under optogenetic-mediated specific activation patterns. Here, we show that GRAB_{sNPFL0} and ACh3.0 can be used to determine the optogenetic parameters needed to trigger the in vivo release of sNPF and ACh, respectively, in the *Drosophila* MB. Notably, trains of optogenetic pulses induced a potentiation of sNPF release, but caused a depression in ACh release, suggesting that distinct processes may underlie the regulation of various phases during complex behaviors. The post-tetanic potentiation of neuropeptide release was also observed in larval *Drosophila* neuromuscular junctions¹⁰⁶. And further studies revealed that CaMKII and the Ryanodine receptor play pivotal roles in modulating this pattern^{106,107}. This finding aligned with the distinct localization patterns of LDCVs and SVs, where SVs tend to cluster near the active zone, while LDCVs are dispersed in remote regions away from the active zone^{103,108}.

Molecular regulation of neuropeptide release

The Syt family is highly conserved across different species, with *Drosophila* Syt1 and Syt7 being orthologous to the mouse Syt1 and Syt7



genes respectively, furthermore, *Drosophila* Syt α shares the highest similarity to mouse Syt9, Syt10, and Syt3⁹⁹. Despite decades of study, the function of most Syt isoforms with respect to the release of neuropeptides remains poorly understood. To address this question, we systematically screened all five putative Ca²⁺-sensitive Syt isoforms for their role in mediating neuropeptide release in the *Drosophila* MB and

found that both Syt α and Syt7 are required for sNPF release. It was correlated well with previous reports, such as Park et al. reported that knocking down Syt α using RNAi mimicked the phenotype associated with loss of the bioactive peptides PETH and ETH (pre-ecdyss and ecdysis-triggering hormones, respectively) from Inka cells in *Drosophila*, suggesting that the Syt α contribute to neuropeptide release

Fig. 6 | The GRAB_{sNPF_{L0}} and ACh3.0 sensors reveal distinct differences in the molecular control of sNPF and ACh release in flies. **a** Left, schematic diagram depicting the release of sNPF via nSyb. Representative pseudocolor images and traces (middle), the summary peak $\Delta F/F_0$ (Right) of GRAB_{sNPF_{L0}}. High K⁺ application: $n = 10$ flies for Ctrl, $n = 9$ flies for Tetzlc; sNPF application: $n = 9$ for Ctrl and Tetzlc. Two-tailed Student's t tests, High K⁺ application, $P = 2.17 \times 10^{-5}$ for Ctrl versus Tetzlc; sNPF application: $P = 0.75$ for Ctrl versus Tetzlc. **b** Left, schematic diagram depicting the release of ACh via nSyb. Representative pseudocolor images and traces (middle), the summary (right) peak $\Delta F/F_0$ of ACh3.0. 1 Hz 10 s: $n = 5$ flies for Ctrl and Tetzlc; ACh application: $n = 5$ flies for Ctrl, $n = 4$ flies for Tetzlc. Two-tailed Student's t tests, High K⁺ application, $P = 9.08 \times 10^{-5}$ for Ctrl versus Tetzlc; sNPF application: $P = 0.24$ for Ctrl versus Tetzlc. Left, schematic diagrams depicting the

release of sNPF (c) and ACh (d) via synaptotagmins (Syts). Also shown are representative fluorescence images (top right) and pseudocolor images (middle right), and traces (bottom right) of GRAB_{sNPF_{L0}} (c) and ACh3.0 (d) response. Summary of the peak $\Delta F/F_0$ of GRAB_{sNPF_{L0}} (e) and ACh3.0 (f). For GRAB_{sNPF_{L0}}, $n = 8, 6, 5, 9, 9, 7$ flies for Ctrl, sg-Syt1, sg-Syt4, sg-Syt7, sg-Syt α , sg-Syt β . For ACh3.0, $n = 8, 9, 6, 6, 7, 6$ flies for Ctrl, sg-Syt1, sg-Syt4, sg-Syt7, sg-Syt α , sg-Syt β . One-way ANOVA followed by Tukey's multiple-comparison test, e $F_{5,38} = 8.75$, $P = 1.36 \times 10^{-6}$. Post hoc test: $P = 1.79 \times 10^{-3}$ for Ctrl versus sg-Syt7, $P = 4.34 \times 10^{-3}$ for Ctrl versus sg-Syt α . f $F_{5,36} = 11.81$, $P = 8.4 \times 10^{-7}$. Post hoc test: $P = 5.85 \times 10^{-4}$ for Ctrl versus sg-Syt1. **g** Model depicting the molecular regulation of sNPF and ACh release. All Scale bar, 25 μm . Data are shown as mean \pm s.e.m. in a–f, with the error bars or shaded regions indicating the s.e.m. *** $P < 0.001$, ** $P < 0.01$, and n.s. not significant.

from neuroendocrine cells¹⁰⁹. In addition, Seibert et al. recently reported that Syt9 may be required for the release of substance P from dense-core vesicles (DCVs) in striatal neurons in vertebrates⁹⁸. Notably, both Syt1 and Syt7 are reported to play a role in DCV fusion in hippocampal neurons¹¹⁰, suggesting they may have multiple roles in regulating neurosecretion. We found that Syt1 mediates the fast ACh release and Syt7/Syt α mediates the slow sNPF release. Similarly, it has been shown in mouse neurons that Syt1 and Syt7 mediate the synchronous (fast) and asynchronous (slow) glutamate release, respectively⁹⁵. Interestingly, Syt4, which does not contain a Ca²⁺-binding site, has been shown to negatively regulate the release of brain-derived neurotrophic factor (BDNF)¹¹¹, while Syt10, which does contain a Ca²⁺-binding site, positively regulates the release of insulin-like growth factor 1 (IGF-1) from DCVs in neurons¹¹². Together with our findings, these results support the notion that Syts have divergent roles and are involved in controlling distinct secretion pathways in neurons, depending on the specific cell type. Moreover, our results provide direct evidence that two Syt isoforms mediate neuropeptide release in *Drosophila*.

Why two Syt isoforms are required for the release of sNPF in the same neuron remains unclear. However, one possible explanation is that these two Syt isoforms function in the same secretory pathway. In this respect, it is interesting to note that previous studies suggested that Syt α may be localized to LDCVs¹⁰⁹, while Syt7 may be localized primarily to the peri-active zone⁹⁷, and the results of Syt7 and Syt α double knock out also supports this conclusion. Regarding the remaining release after double knock-out, we speculate that this occurs because the CRISPR-Cas9-sgRNA mediated knock-out efficiency does not reach 100%. Still, we could not rule out the possibility that other calcium sensors might regulate neuropeptide release.

In conclusion, our study demonstrates that the GRAB_{sNPF_{L0}} sensor is a robust tool for monitoring sNPF release in vivo with high specificity and spatiotemporal resolution. Our findings regarding the dynamics and molecular regulation of sNPF and ACh release provide valuable insights into the complex mechanisms by which neuropeptides and small molecule neurotransmitters are released from the same type of neurons.

Methods

Molecular cloning

The plasmids used in this study were generated using the Gibson assembly method. DNA inserts were generated by PCR amplification using primers (RuiBiotech) with -25-bp overlap, and all sequences were verified using Sanger sequencing (RuiBiotech). All cDNAs encoding the candidate GRAB_{sNPF} sensors were cloned into the pDisplay vector (Invitrogen) with an upstream IgK leader sequence and a downstream IRES-mCherry-CAAX cassette (to visualize localization to the cell membrane). For screening replacement sites, cDNAs encoding the various sNPF receptors were generated (Shang Genegay Biotech), and the third intracellular loop (ICL3) of each sNPF receptor was replaced with the corresponding ICL3 in GRAB_{NEIm}. For optimizing the sNPF sensor, we screened the replaced sites in the *Culex* sNPF receptor, the

amino acid composition between the *Culex* sNPF receptor and the ICL3 of GRAB_{NEIm}, and cpEGFP. Site-directed mutagenesis was performed using primers containing randomized NNB codons (48 codons in total, encoding all 20 amino acids) or defined codons at the target sites.

Cell lines

HEK293T cells were acquired from ATCC (Supplementary Data 1) and verified by microscopic examination of their morphology and growth curve. An HTLA cell line stably expressing a tTA-dependent luciferase reporter and the β -arrestin2-TEV fusion gene used in the Tango assay was a generous gift from Bryan L. Roth (University of North Carolina Chapel Hill, Supplementary Data 1). The cells were cultured in DMEM (Biological Industries) supplemented with 10% (v/v) fetal bovine serum (FBS, Gibco) and 1% penicillin-streptomycin (Gibco) at 37 °C in humidified air containing 5% CO₂.

Fly strain generation and animal husbandry

In this study, we generated UAS-GRAB_{sNPF_{L0}} (attp40, UAS-GRAB_{sNPF_{L0}}/CyO), UAS-GRAB_{sNPF_{L0}} (vk00005, UAS-GRAB_{sNPF_{L0}}/TM2), and UAS-GRAB_{sNPF_{mut}} (attp40, UAS-GRAB_{sNPF_{mut}}/CyO) vectors using Gibson assembly to integrate the coding sequence of GRAB_{sNPF_{L0}} into the pJFRC28 (Addgene plasmid 36431) or modified pJFRC28 vector.

The UAS-Syt1-sgRNA, UAS-Syt4-sgRNA, UAS-Syt7-sgRNA, UAS-Syt α -sgRNA, and UAS-Syt β -sgRNA constructs were designed by inserting three guide RNAs (sgRNAs) into the pMsgNull vector based on pACU2 (Addgene #31223)¹¹³ (From Dr. Yi Rao lab at Peking University), with rice transfer RNA (tRNA) used to separate the various sgRNAs. The resulting vectors were then injected into embryos and integrated into attp40 or vk00005 via phiC31 by the Core Facility of *Drosophila* Resource and Technology, Shanghai Institute of Biochemistry and Cell Biology, Chinese Academy of Sciences. For each Syt isoform, the following guide sequences are used: Syt1: CGAGGTGATCGCGGAGCGCA, TCGGTGAGTTCTCCATATC, GTATAATCTTCTTGTGTG; Syt4: CCGGAACCCGGTTTACGACG, CGATCGTCTCTACCGGCGAG, AGGGGAACGAGGCGTCGTGC; Syt7: TTTCAAGAGATGACTCCATA, CTAATGACAGACATGTATT, GCATGTGCCACCGGCAC TTG; Syt α : AGAGGCATAGACGCCAATT, ATCCAGCTTGGCGTTCA-TAG, GTTCACTCAACGAAGTTCG; Syt β : GATCAGGGCCAATCTG-TAC, GAGGCTCTTACCACAGATA, GGAGCTGATCCCGGAGAACC.

The flies were raised on standard corn meal-yeast medium at 25 °C in 50% relative humidity under a 12 h/12 h light/dark cycle. For optogenetics, after eclosion, the flies were transferred to corn meal containing 400 μM all-*trans*-retinal and raised in the dark for 1–3 days before performing functional imaging experiments.

All experiments were conducted using the fruit fly species *Drosophila melanogaster*. The transgenic lines employed in this study are listed in Supplementary Data 1.

Fluorescence imaging of HEK 293T cells

Cells were imaged using an inverted Ti-E A1 confocal microscope (Nikon) or an Opera Phenix high-content screening system

(PerkinElmer). The confocal microscope was equipped with a 10×/0.45 NA (numerical aperture) objective, a 20×/0.75 NA objective, a 40×/1.35 NA oil-immersion objective, a 488-nm laser, and a 561-nm laser; the GFP signal was collected using a 525/50-nm emission filter combined with the 488-nm laser, and the RFP signal was collected using a 595/50-nm emission filter combined with the 561-nm laser. The Opera Phenix system was equipped with 20×/0.4 NA objective, a 40×/1.1 NA water-immersion objective, a 488-nm laser, and a 561-nm laser; the GFP and RFP signals were collected using a 525/50-nm and 600/30-nm emission filter, respectively. The fluorescence signal produced by the green fluorescent GRAB_{sNPF} sensors was calibrated using the GFP/RFP ratio.

HEK293T cells were plated on either 12-mm glass coverslips in 24-well plates or 96-well plates and grown to ~70% confluence for transfection with PEI (1 µg plasmid and 3 µg PEI per well in 24-well plates or 300 ng plasmids and 900 ng PEI per well in 96-well plates); the medium was replaced after 4–6 h, and the cells were used for imaging 24–48 h after transfection. To measure the kinetics of the GRAB_{sNPF} sensor, the confocal high-speed line scanning mode (512 Hz) was used to measure the fluorescence signal change when the cells were locally puffed with sNPF via a glass pipette positioned in close proximity to the cells, the increased and decreased trace in fluorescence was fitted with a single-exponential function. The off kinetics were determined through a wash-out procedure conducted at room temperature, which was approximately 20 °C. Additionally, both *in vivo* and *in vitro* imaging experiments were carried out under identical temperature conditions, specifically at approximately 20 °C.

The synthesized peptide powder was stored in –20 °C, and dissolved in sterile water upon utilization. The compounds used in this study are listed in Supplementary Data 1.

Tango assay

HTLA cells were cultured in 6-well plates; at ~70% cell density, the cells were transfected with either wild-type *Culex* sNPF or the GRAB_{sNPFLO}. Twenty-four hours after transfection, the cells were transferred to a 96-well white clear flat-bottom plate, and various concentrations of sNPF (ranging from 0.1 nM to 5 µM) were added to the cells; each concentration was applied in triplicate. The cells were then incubated for ~16 h, and the bioluminescent signal was measured. To measure the bioluminescent signal, the culture medium was removed, and 40 µl of Bright-Glo substrate (Promega) was added to each well. The plate was then incubated at room temperature in the dark for 10 min, and bioluminescence was measured using a Victor X5 microplate reader (PerkinElmer). Non-transfected cells were used as a negative control.

Luciferase complementation assay

The luciferase complementation assay was performed as previously described¹¹⁴. In brief, 24–48 h after transfection, the cells were washed with PBS, dissociated using a cell scraper, resuspended in PBS, transferred to opaque 96-well plates containing 5 µM furimazine (NanoLuc Luciferase Assay, Promega), and bathed in sNPF at various concentrations (ranging from 0.1 nM to 5 µM). After incubation for 10 minutes in the dark, luminescence was measured using a Victor X5 microplate reader (PerkinElmer).

Spectra measurements

For one-photon spectra, HEK293T cells were transfected with CMV promoter-driven GRAB_{sNPFLO} plasmids; after 24 h, the cells were harvested and transferred to a 384-well plate in the absence or presence of 1 µM sNPF. Excitation and emission spectra were measured at 5-nm increments with a 20-nm bandwidth using a Safire2 multi-mode plate reader (Tecan). For background subtraction, non-transfected cells were prepared and measured using the same protocol.

For two-photon spectra, cells were transfected with GRAB_{sNPFLO} and treated as described above. Excitation and emission spectra were

measured from 700 nm to 1020 nm at 10-nm increments using an FV1000 two-photon microscope (Olympus) equipped with a Spectra-Physics Mai Tai Ti:Sapphire laser. Non-transfected cells were used to subtract the background signal.

Two-photon imaging of flies

Fluorescence imaging in flies was performed using an FV1000 two-photon microscope (Olympus) equipped with a Spectra-Physics Mai Tai Ti:Sapphire laser. A 920-nm excitation laser was used for one-color imaging of GRAB_{sNPFLO} and GRAB_{sNPFmut}, and a 950-nm excitation laser was used for two-color imaging of GRAB_{sNPFLO} and mCherry or GRAB_{sNPFLO} and rACh0.5. For detection, a 495–540-nm filter was used for the green channel, and a 575–630-nm filter was used for red channel. Adult female flies were used for imaging within 1 week after eclosion. To prepare the fly for imaging, adhesive tape was affixed to the head and wings. The tape above the head was excised, and the chitin head-shell, air sacs, and fat bodies were carefully removed to expose the central brain. The brain was bathed continuously in an adult hemolymph-like solution composed of (in mM): 108 NaCl, 5 KCl, 5 HEPES, 5 trehalose, 5 sucrose, 26 NaHCO₃, 1 NaH₂PO₄, 2 CaCl₂, and 1–2 MgCl₂. For single-photon optogenetic stimulation, a 635-nm laser (Changchun Liangli Photo Electricity Co., Ltd.) was used, and 18 mW/cm² light pulses were delivered to the brain via an optic fiber. For the perfusion experiments, a small section of the blood-brain-barrier was carefully removed with tweezers before applying the indicated compounds or solutions. Detailed fly genotypes corresponding to each figure are listed in Supplementary Data 2.

Statistics & reproducibility

Images were processed using ImageJ software (National Institutes of Health). The change in fluorescence ($\Delta F/F_0$) was calculated using the formula $[(F - F_0)/F_0]$, where F_0 represents the baseline fluorescence. The signal-to-noise ratio (SNR) was calculated by dividing the peak response by the standard deviation of the baseline fluorescence. The area under the curve was determined using the integral of the change in fluorescence ($\int \Delta F/F_0$).

Origin 2019 (OriginLab) was used to perform the statistical analyses. Unless otherwise specified, all summary data are presented as the mean ± sem. The paired or unpaired Student's *t* test was used to compare two groups, and a one-way analysis of variance (ANOVA) with Tukey's multiple-comparison tests was used to compare more than two groups. All statistical tests were two-tailed, and differences were considered statistically significant at $P < 0.05$. No statistical method was used to predetermine sample size. No data were excluded from the analysis. Additionally, the experiments were not randomized and the Investigators were not blinded to allocation during experiments and outcome assessment. For all representative images and traces, similar results were obtained for >3 independent experiments.

Reporting summary

Further information on research design is available in the Nature Portfolio Reporting Summary linked to this article.

Data availability

Protein sequences for the sensors developed in this study are available in Supplementary Fig. 1. DNA sequences for the sensors developed in this study are available in Supplementary Data 3. Source data are provided with this paper.

Code availability

The custom-written python, Arduino, and Image J programs are available in the Zenodo database under accession code digital object identifier: 10.5281/zenodo.14405339 (<https://zenodo.org/records/14405339>)¹¹⁵.

References

1. van den Pol, A. N. Neuropeptide transmission in brain circuits. *Neuron* **76**, 98–115 (2012).
2. Hyman, S. E. Neurotransmitters. *Curr. Biol.* **15**, R154–R158 (2005).
3. Nusbaum, M. P., Blitz, D. M. & Marder, E. Functional consequences of neuropeptide and small-molecule co-transmission. *Nat. Rev. Neurosci.* **18**, 389–403 (2017).
4. Nassel, D. R. Substrates for Neuronal Cotransmission With Neuropeptides and Small Molecule Neurotransmitters in *Drosophila*. *Front. Cell Neurosci.* **12**, 83 (2018).
5. Schone, C., Apergis-Schoute, J., Sakurai, T., Adamantidis, A. & Burdakov, D. Coreleased orexin and glutamate evoke non-redundant spike outputs and computations in histamine neurons. *Cell Rep.* **7**, 697–704 (2014).
6. Decamilli, P. & Jahn, R. Pathways to Regulated Exocytosis in Neurons. *Annu. Rev. Physiol.* **52**, 625–645 (1990).
7. Svensson, E. et al. General Principles of Neuronal Co-transmission: Insights From Multiple Model Systems. *Front. Neural Circuits* **12**, 117 (2019).
8. Florman, J. T. & Alkema, M. J. Co-transmission of neuropeptides and monoamines choreograph the *C. elegans* escape response. *PLoS Genet.* **18**, e1010091 (2022).
9. Jan, Y. N., Jan, L. Y. & Kuffler, S. W. Further evidence for peptidergic transmission in sympathetic ganglia. *Proc. Natl Acad. Sci. USA* **77**, 5008–5012 (1980).
10. Smith, S. J. et al. Single-cell transcriptomic evidence for dense intracortical neuropeptide networks. *eLife* **8**, e47889 (2019).
11. Root, C. M., Ko, K. I., Jafari, A. & Wang, J. W. Presynaptic facilitation by neuropeptide signaling mediates odor-driven food search. *Cell* **145**, 133–144 (2011).
12. Hokfelt, T. et al. Neuropeptide and Small Transmitter Coexistence: Fundamental Studies and Relevance to Mental Illness. *Front. Neural Circuits* **12**, 106 (2018).
13. Xie, Z. et al. The gut-to-brain axis for toxin-induced defensive responses. *Cell* **185**, 4298–4316.e4221 (2022).
14. Soden, M. E., Yee, J. X. & Zweifel, L. S. Circuit coordination of opposing neuropeptide and neurotransmitter signals. *Nature* **619**, 332–337 (2023).
15. Nassel, D. R. & Zandawala, M. Recent advances in neuropeptide signaling in *Drosophila*, from genes to physiology and behavior. *Prog. Neurobiol.* **179**, 101607 (2019).
16. Nassel, D. R., Pauls, D. & Huetteroth, W. Neuropeptides in modulation of *Drosophila* behavior: how to get a grip on their pleiotropic actions. *Curr. Opin. Insect Sci.* **36**, 1–8 (2019).
17. Chen, W. et al. Regulation of sleep by the short neuropeptide F (sNPF) in *Drosophila melanogaster*. *Insect. Biochem. Mol. Biol.* **43**, 809–819 (2013).
18. Shang, Y. et al. Short neuropeptide F is a sleep-promoting inhibitory modulator. *Neuron* **80**, 171–183 (2013).
19. Nassel, D. R. & Wegener, C. A comparative review of short and long neuropeptide F signaling in invertebrates: Any similarities to vertebrate neuropeptide Y signaling? *Peptides* **32**, 1335–1355 (2011).
20. Nassel, D. R., Enell, L. E., Santos, J. G., Wegener, C. & Johard, H. A. D. A large population of diverse neurons in the *Drosophila* central nervous system expresses short neuropeptide F, suggesting multiple distributed peptide functions. *BMC Neurosci.* **9**, 90 (2008).
21. Oh, Y. et al. A glucose-sensing neuron pair regulates insulin and glucagon in *Drosophila*. *Nature* **574**, 559–564 (2019).
22. Lee, K.-S. et al. *Drosophila* short neuropeptide F signalling regulates growth by ERK-mediated insulin signalling. *Nat. Cell Biol.* **10**, 468–475 (2008).
23. Croset, V., Treiber, C. D. & Waddell, S. Cellular diversity in the *Drosophila* midbrain revealed by single-cell transcriptomics. *eLife* **7**, e34550 (2018).
24. Barnstedt, O. et al. Memory-Relevant Mushroom Body Output Synapses Are Cholinergic. *Neuron* **89**, 1237–1247 (2016).
25. Johard, H. A. D. et al. Intrinsic neurons of *Drosophila* mushroom bodies express short neuropeptide F: relations to extrinsic neurons expressing different neurotransmitters. *J. Comp. Neurol.* **507**, 1479–1496 (2008).
26. Deng, B. et al. Chemoconnectomics: Mapping Chemical Transmission in *Drosophila*. *Neuron* **101**, 876–893.e874 (2019).
27. Knapek, S., Kahsai, L., Winther, A. M., Tanimoto, H. & Nassel, D. R. Short neuropeptide F acts as a functional neuromodulator for olfactory memory in Kenyon cells of *Drosophila* mushroom bodies. *J. Neurosci.* **33**, 5340–5345 (2013).
28. Lyutova, R. et al. Reward signaling in a recurrent circuit of dopaminergic neurons and peptidergic Kenyon cells. *Nat. Commun.* **10**, 3097 (2019).
29. Jing, M. et al. An optimized acetylcholine sensor for monitoring in vivo cholinergic activity. *Nat. Methods* **17**, 1139–1146 (2020).
30. Zeng, J. et al. Local 5-HT signaling bi-directionally regulates the coincidence time window for associative learning. *Neuron* **111**, 1118–1135.e1115 (2023).
31. Kendrick, K. M. Microdialysis measurement of in vivo neuropeptide release. *J. Neurosci. Methods* **34**, 35–46 (1990).
32. Burke, N. V. et al. Neuronal peptide release is limited by secretory granule mobility. *Neuron* **19**, 1095–1102 (1997).
33. Zhu, D. et al. Synaptotagmin I and IX function redundantly in controlling fusion pore of large dense core vesicles. *Biochem. Biophys. Res. Commun.* **361**, 922–927 (2007).
34. Ding, K. et al. Imaging neuropeptide release at synapses with a genetically engineered reporter. *eLife* **8**, e46421 (2019).
35. Bulgari, D. et al. Activity-evoked and spontaneous opening of synaptic fusion pores. *Proc. Natl Acad. Sci. USA* **116**, 17039–17044 (2019).
36. Kim, D.-I. et al. Presynaptic sensor and silencer of peptidergic transmission reveal neuropeptides as primary transmitters in pontine fear circuit. *Cell* **187**, 5102–5117.e5116 (2024).
37. Barnea, G. et al. The genetic design of signaling cascades to record receptor activation. *Proc. Natl Acad. Sci. USA* **105**, 64–69 (2008).
38. Lee, D. et al. Temporally precise labeling and control of neuromodulatory circuits in the mammalian brain. *Nat. Methods* **14**, 495–503 (2017).
39. Inagaki, H. K. et al. Visualizing Neuromodulation In Vivo: TANGO-Mapping of Dopamine Signaling Reveals Appetite Control of Sugar Sensing. *Cell* **148**, 583–595 (2012).
40. Jones, J. R., Simon, T., Lones, L. & Herzog, E. D. SCN VIP Neurons Are Essential for Normal Light-Mediated Resetting of the Circadian System. *J. Neurosci.* **38**, 7986–7995 (2018).
41. Pinol, R. A., Jameson, H., Popratiloff, A., Lee, N. H. & Mendelowitz, D. Visualization of Oxytocin Release that Mediates Paired Pulse Facilitation in Hypothalamic Pathways to Brainstem Autonomic Neurons. *Plos One* **9**, e112138 (2014).
42. Pitra, S., Zhang, M., Cauley, E. & Stern, J. E. NMDA receptors potentiate activity-dependent dendritic release of neuropeptides from hypothalamic neurons. *J. Physiol.* **597**, 1735–1756 (2019).
43. Xiong, H. J. et al. Probing Neuropeptide Volume Transmission In Vivo by Simultaneous Near-Infrared Light-Triggered Release and Optical Sensing. *Angew. Chem. Int. Ed.* **61**, e202206122 (2022).
44. Muller, A., Joseph, V., Slesinger, P. A. & Kleinfeld, D. Cell-based reporters reveal in vivo dynamics of dopamine and nor-epinephrine release in murine cortex. *Nat. Methods* **11**, 1245–1252 (2014).
45. Sun, F. et al. A Genetically Encoded Fluorescent Sensor Enables Rapid and Specific Detection of Dopamine in Flies, Fish, and Mice. *Cell* **174**, 481–496.e419 (2018).

46. Jing, M. et al. A genetically encoded fluorescent acetylcholine indicator for in vitro and in vivo studies. *Nat. Biotechnol.* **36**, 726–737 (2018).
47. Patriarchi, T. et al. Ultrafast neuronal imaging of dopamine dynamics with designed genetically encoded sensors. *Science* **360**, eaat4422 (2018).
48. Feng, J. et al. A Genetically Encoded Fluorescent Sensor for Rapid and Specific In Vivo Detection of Norepinephrine. *Neuron* **102**, 745–761 e748 (2019).
49. Wan, J. et al. A genetically encoded sensor for measuring serotonin dynamics. *Nat. Neurosci.* **24**, 746–752 (2021).
50. Wu, Z. et al. A sensitive GRAB sensor for detecting extracellular ATP in vitro and in vivo. *Neuron* **110**, 770–782 (2021).
51. Duffet, L. et al. A genetically encoded sensor for in vivo imaging of orexin neuropeptides. *Nat. Methods* **19**, 231–241 (2022).
52. Qian, T. R. et al. A genetically encoded sensor measures temporal oxytocin release from different neuronal compartments. *Nat. Biotechnol.* **41**, 944–957 (2023).
53. Sun, F. et al. Next-generation GRAB sensors for monitoring dopaminergic activity in vivo. *Nat. Methods* **17**, 1156–1166 (2020).
54. Ino, D., Tanaka, Y., Hibino, H. & Nishiyama, M. A fluorescent sensor for real-time measurement of extracellular oxytocin dynamics in the brain. *Nat. Methods* **19**, 1286–1294 (2022).
55. Wu, Z. et al. Neuronal activity-induced, equilibrative nucleoside transporter-dependent, somatodendritic adenosine release revealed by a GRAB sensor. *Proc. Natl Acad. Sci.* **120**, e2212387120 (2023).
56. Peng, W. et al. Regulation of sleep homeostasis mediator adenosine by basal forebrain glutamatergic neurons. *Science* **369**, eabb0556 (2020).
57. Dong, H. et al. Genetically encoded sensors for measuring histamine release both in vitro and in vivo. *Neuron*, **111**, 1564–1576.e6 (2023).
58. Patriarchi, T. et al. An expanded palette of dopamine sensors for multiplex imaging in vivo. *Nat. Methods* **17**, 1147–1155 (2020).
59. Dong, A. et al. A fluorescent sensor for spatiotemporally resolved imaging of endocannabinoid dynamics in vivo. *Nat. Biotechnol.* **40**, 787–798 (2021).
60. Wang, H. et al. A tool kit of highly selective and sensitive genetically encoded neuropeptide sensors. *Science* **382**, eabq8173 (2023).
61. Dong, C. et al. Unlocking opioid neuropeptide dynamics with genetically encoded biosensors. *Nat. Neurosci.* **27**, 1844–1857 (2024).
62. Zhou, X. et al. Development of a genetically encoded sensor for probing endogenous nociceptin opioid peptide release. *Nat. Commun.* **15**, 5353 (2024).
63. Cola, R. B. et al. Probing PAC1 receptor activation across species with an engineered sensor. *eLife* **13**, RP96496 (2024).
64. Christ, P., Hill, S. R., Schachtner, J., Hauser, F. & Ignell, R. Functional characterization of mosquito short neuropeptide F receptors. *Peptides* **103**, 31–39 (2018).
65. Mertens, I., Meeusen, T., Huybrechts, R., De Loof, A. & Schoofs, L. Characterization of the short neuropeptide F receptor from *Drosophila melanogaster*. *Biochem. Biophys. Res. Commun.* **297**, 1140–1148 (2002).
66. Lee, K.-S. et al. Processed short neuropeptide F peptides regulate growth through the ERK-insulin pathway in *Drosophila melanogaster*. *FEBS Lett.* **583**, 2573–2577 (2009).
67. Reale, V., Chatwin, H. M. & Evans, P. D. The activation of G-protein gated inwardly rectifying K⁺ channels by a cloned *Drosophila melanogaster* neuropeptide F-like receptor. *Eur. J. Neurosci.* **19**, 570–576 (2004).
68. Liang, X., Holy, T. E. & Taghert, P. H. A Series of Suppressive Signals within the *Drosophila* Circadian Neural Circuit Generates Sequential Daily Outputs. *Neuron* **94**, 1173–1189.e1174 (2017).
69. Yang, Z. et al. Structural basis of ligand binding modes at the neuropeptide Y Y1 receptor. *Nature* **556**, 520–524 (2018).
70. Vanden Broeck, J. Neuropeptides and their precursors in the fruitfly, *Drosophila melanogaster*. *Peptides* **22**, 241–254 (2001).
71. Baggerman, G., Cerstiaens, A., De Loof, A. & Schoofs, L. Peptidomics of the larval *Drosophila melanogaster* central nervous system. *J. Biol. Chem.* **277**, 40368–40374 (2002).
72. Predel, R. et al. Peptidomics of CNS-associated neurohemal systems of adult *Drosophila melanogaster*: a mass spectrometric survey of peptides from individual flies. *J. Comp. Neurol.* **474**, 379–392 (2004).
73. Baggerman, G., Boonen, K., Verleyen, P., De Loof, A. & Schoofs, L. Peptidomic analysis of the larval *Drosophila melanogaster* central nervous system by two-dimensional capillary liquid chromatography quadrupole time-of-flight mass spectrometry. *J. Mass Spectrom.* **40**, 250–260 (2005).
74. Yew, J. Y. et al. Analysis of neuropeptide expression and localization in adult *Drosophila melanogaster* central nervous system by affinity cell-capture mass spectrometry. *J. Proteome Res.* **8**, 1271–1284 (2009).
75. Aso, Y. et al. Nitric oxide acts as a cotransmitter in a subset of dopaminergic neurons to diversify memory dynamics. *eLife* **8**, e49257 (2019).
76. Klapoetke, N. C. et al. Independent optical excitation of distinct neural populations. *Nat. Methods* **11**, 338–346 (2014).
77. Barg, S. et al. Delay between fusion pore opening and peptide release from large dense-core vesicles in neuroendocrine cells. *Neuron* **33**, 287–299 (2002).
78. Zucker, R. S. & Regehr, W. G. Short-term synaptic plasticity. *Annu. Rev. Physiol.* **64**, 355–405 (2002).
79. Citri, A. & Malenka, R. C. Synaptic plasticity: multiple forms, functions, and mechanisms. *Neuropsychopharmacology* **33**, 18–41 (2008).
80. Zhang, Y. et al. Interaction of acetylcholine and oxytocin neuromodulation in the hippocampus. *Neuron* **112**, 1862–1875.e1865 (2024).
81. Alabi, A. A. & Tsien, R. W. Synaptic vesicle pools and dynamics. *Cold Spring Harb. Perspect. Biol.* **4**, a013680 (2012).
82. Sudhof, T. C. & Rothman, J. E. Membrane Fusion: Grappling with SNARE and SM Proteins. *Science* **323**, 474–477 (2009).
83. Kasai, H., Takahashi, N. & Tokumaru, H. Distinct Initial Snare Configurations Underlying the Diversity of Exocytosis. *Physiological Rev.* **92**, 1915–1964 (2012).
84. Deitcher, D. L. et al. Distinct requirements for evoked and spontaneous release of neurotransmitter are revealed by mutations in the *Drosophila* gene neuronal-synaptobrevin. *J. Neurosci.* **18**, 2028–2039 (1998).
85. Sweeney, S. T., Broadie, K., Keane, J., Niemann, H. & O’Kane, C. J. Targeted expression of tetanus toxin light chain in *Drosophila* specifically eliminates synaptic transmission and causes behavioral defects. *Neuron* **14**, 341–351 (1995).
86. Sudhof, T. C. Calcium Control of Neurotransmitter Release. *Cold Spring Harb. Perspect. Biol.* **4**, a011353 (2012).
87. Rizo, J. Molecular Mechanisms Underlying Neurotransmitter Release. *Annu. Rev. Biophys.* **51**, 377–408 (2022).
88. Sudhof, T. C. Neurotransmitter Release: The Last Millisecond in the Life of a Synaptic Vesicle. *Neuron* **80**, 675–690 (2013).
89. Littleton, J. T., Stern, M., Schulze, K., Perin, M. & Bellen, H. J. Mutational Analysis of *Drosophila* Synaptotagmin Demonstrates Its Essential Role in Ca²⁺-Activated Neurotransmitter Release. *Cell* **74**, 1125–1134 (1993).

90. Diantonio, A., Parfitt, K. D. & Schwarz, T. L. Synaptic Transmission Persists in Synaptotagmin Mutants of *Drosophila*. *Cell* **73**, 1281–1290 (1993).
91. Geppert, M. et al. Synaptotagmin-I - a Major Ca²⁺ Sensor for Transmitter Release at a Central Synapse. *Cell* **79**, 717–727 (1994).
92. Fernandez-Chacon, R. et al. Synaptotagmin I functions as a calcium regulator of release probability. *Nature* **410**, 41–49 (2001).
93. Tang, J. et al. A complexin/synaptotagmin 1 switch controls fast synaptic vesicle exocytosis. *Cell* **126**, 1175–1187 (2006).
94. Xu, J., Mashimo, T. & Sudhof, T. C. Synaptotagmin-1,-2, and-9: Ca²⁺ sensors for fast release that specify distinct presynaptic properties in subsets of neurons. *Neuron* **54**, 567–581 (2007).
95. Bacaj, T. et al. Synaptotagmin-1 and Synaptotagmin-7 Trigger Synchronous and Asynchronous Phases of Neurotransmitter Release. *Neuron* **80**, 947–959 (2013).
96. Bacaj, T. et al. Synaptotagmin-1 and -7 Are Redundantly Essential for Maintaining the Capacity of the Readily-Releasable Pool of Synaptic Vesicles. *PLOS Biol.* **13**, e1002267 (2015).
97. Guan, Z., Quinones-Frias, M. C., Akbergenova, Y. & Littleton, J. T. *Drosophila* Synaptotagmin 7 negatively regulates synaptic vesicle release and replenishment in a dosage-dependent manner. *eLife* **9**, e55443 (2020).
98. Seibert, M. J., Evans, C. S., Stanley, K. S., Wu, Z. & Chapman, E. R. Synaptotagmin 9 Modulates Spontaneous Neurotransmitter Release in Striatal Neurons by Regulating Substance P Secretion. *J. Neurosci.* **43**, 1475–1491 (2023).
99. Quiñones-Frías, M. C. & Littleton, J. T. Function of *Drosophila* Synaptotagmins in membrane trafficking at synapses. *Cell. Mol. Life Sci.* **78**, 4335–4364 (2021).
100. Port, F. & Bullock, S. L. Augmenting CRISPR applications in *Drosophila* with tRNA-flanked sgRNAs. *Nat. Methods* **13**, 852–854 (2016).
101. Ludwig, M. & Leng, G. Dendritic peptide release and peptide-dependent behaviours. *Nat. Rev. Neurosci.* **7**, 126–136 (2006).
102. Klose, M. K., Bruchez, M. P., Deitcher, D. L. & Levitan, E. S. Temporally and spatially partitioned neuropeptide release from individual clock neurons. *Proc. Natl Acad. Sci. USA* **118**, e2101818118 (2021).
103. Hofbauer, B. et al. The neuropeptide pigment-dispersing factor signals independently of Bruchpilot-labelled active zones in daily remodelled terminals of *Drosophila* clock neurons. *Eur. J. Neurosci.* **59**, 2665–2685 (2024).
104. Anthony. Neuropeptide Transmission in Brain Circuits. *Neuron* **76**, 98–115 (2012).
105. Hui, E. et al. Three distinct kinetic groupings of the synaptotagmin family: candidate sensors for rapid and delayed exocytosis. *Proc. Natl Acad. Sci. USA* **102**, 5210–5214 (2005).
106. Shakiryanova, D., Tully, A., Hewes, R. S., Deitcher, D. L. & Levitan, E. S. Activity-dependent liberation of synaptic neuropeptide vesicles. *Nat. Neurosci.* **8**, 173–178 (2005).
107. Shakiryanova, D. et al. Presynaptic ryanodine receptor-activated calmodulin kinase II increases vesicle mobility and potentiates neuropeptide release. *J. Neurosci. Off. J. Soc. Neurosci.* **27**, 7799–7806 (2007).
108. Verhage, M. et al. Differential release of amino acids, neuropeptides, and catecholamines from isolated nerve terminals. *Neuron* **6**, 517–524 (1991).
109. Park, D., Li, P. Y., Dani, A. & Taghert, P. H. Peptidergic Cell-Specific Synaptotagmins in *Drosophila*: Localization to Dense-Core Granules and Regulation by the bHLH Protein DIMMED. *J. Neurosci.* **34**, 13195–13207 (2014).
110. van Westen, R., Poppinga, J., Arazola, R. D., Toonen, R. F. & Verhage, M. Neuromodulator release in neurons requires two functionally redundant calcium sensors. *Proc. Natl Acad. Sci. USA* **118**, e2012137118 (2021).
111. Dean, C. et al. Synaptotagmin-IV modulates synaptic function and long-term potentiation by regulating BDNF release. *Nat. Neurosci.* **12**, 767–2315 (2009).
112. Cao, P., Maximov, A. & Sudhof, T. C. Activity-Dependent IGF-1 Exocytosis Is Controlled by the Ca²⁺-Sensor Synaptotagmin-10. *Cell* **145**, 300–311 (2011).
113. Han, C., Jan, L. Y. & Jan, Y.-N. Enhancer-driven membrane markers for analysis of nonautonomous mechanisms reveal neuron-glia interactions in *Drosophila*. *Proc. Natl Acad. Sci. USA* **108**, 9673–9678 (2011).
114. Wan, Q. W. et al. Mini G protein probes for active G protein-coupled receptors (GPCRs) in live cells. *J. Biol. Chem.* **293**, 7466–7473 (2018).
115. Xia, X. Two-Photon Imaging in *Drosophila*: Codes for Setup and Data Analysis. *Zenodo* <https://doi.org/10.5281/zenodo.14405339> (2024).

Acknowledgements

We thank Yi Rao for providing access to the two-photon microscope. We thank the imaging core facility of State Key Laboratory of Membrane Biology at Peking University (Ye Liang), and Olympus/Evident China Life Science (Shaoling Qi, Wei Cao, Haitao Zhang, Dezhi Zhang, Linliang Yin, and Donghua Wu). We thank Xiaoguang Lei at PKU-CLS and the National Center for Protein Sciences at Peking University for support and assistance with the Opera Phenix high-content screening system. We thank the Core Facility of *Drosophila* Resource and Technology of CAS Center for Excellence in Molecular Cell Science (Wei Wu). We thank members of the Li lab for helpful suggestions and comments on the manuscript. We thank Dr. Man jiang, Dr. Isabel Beets, Dr. Yufeng Pan, Dr. Yan Li, Dr. Xihuimin Dai and Dr. Edwin Levitan for valuable feedback of the manuscript. This work was supported by grants from the Peking-Tsinghua Center for Life Sciences and the State Key Laboratory of Membrane Biology at Peking University School of Life Sciences, the National Natural Science Foundation of China (31925017 and 31871087 to Y.L.), the NIH BRAIN Initiative (NINDS U01NS120824 to Y.L.), the Feng Foundation of Biomedical Research, the Clement and Xinxin Foundation, and the New Cornerstone Science Foundation through the New Cornerstone Investigator Program and the XPLOER PRIZE (to Y.L.).

Author contributions

Y.L. and X.X. designed and supervised the project. X.X. performed and analyzed all experiments. Both authors analyzed and discussed the results. X.X. and Y.L. wrote the manuscript.

Competing interests

The authors declare no competing interests.

Additional information

Supplementary information The online version contains supplementary material available at <https://doi.org/10.1038/s41467-025-56129-w>.

Correspondence and requests for materials should be addressed to Yulong Li.

Peer review information *Nature Communications* thanks the anonymous reviewers for their contribution to the peer review of this work. A peer review file is available.

Reprints and permissions information is available at <http://www.nature.com/reprints>

Publisher's note Springer Nature remains neutral with regard to jurisdictional claims in published maps and institutional affiliations.

Open Access This article is licensed under a Creative Commons Attribution-NonCommercial-NoDerivatives 4.0 International License, which permits any non-commercial use, sharing, distribution and reproduction in any medium or format, as long as you give appropriate credit to the original author(s) and the source, provide a link to the Creative Commons licence, and indicate if you modified the licensed material. You do not have permission under this licence to share adapted material derived from this article or parts of it. The images or other third party material in this article are included in the article's Creative Commons licence, unless indicated otherwise in a credit line to the material. If material is not included in the article's Creative Commons licence and your intended use is not permitted by statutory regulation or exceeds the permitted use, you will need to obtain permission directly from the copyright holder. To view a copy of this licence, visit <http://creativecommons.org/licenses/by-nc-nd/4.0/>.

© The Author(s) 2025